DOI: 10.1002/ejic.200900275

# The Role of Nanostructure in Improving the Performance of Electrodes for Energy Storage and Conversion

**Gabriele Centi*[a] and Siglinda Perathoner[a]**

**Keywords:** Nanostructures / Electrode design / Hierarchical design / Lithium / Fuel cells / Solar cells

The nanostructure is a critical element to improve the performance of electrodes and realize the demanding expectation for a more sustainable and efficient conversion and storage of energy. This microreview analyzes some examples related to advanced electrodes for Li-ion batteries, PEM fuel cells, titania photoanodes and solar cells. The role of a proper nanoarchitecture and hierarchical organization in the electrode, which requires the understanding of the complex physicochemical phenomena occurring at the nanoscale level, is discussed. The need to use cost-effective methods for a robust and scalable preparation is also mentioned. Specific materials and topics discussed are (i) nanostructured carbons (nanotubes and nanofibres, and tube-in-tube materials), (ii) their hybrid nanocomposites with oxides ($TiO_2$, $V_2O_5$), (iii) their use as support for noble metal nanoparticles, and (iv) ordered or non-ordered arrays of titania nanotubes and nanorods.



## 1. Introduction

The need to improve the sustainability and efficiency of the production, storage and use of energy has greatly pushed research interest toward the development of new, improved electrodes with advanced nanoarchitecture.[1–21] There are several key technological areas of the energy sector that require a better design of the electrode nanostructure to overcome current limits and/or move to new levels of their performance: (i) photoelectrochemical solar cells, (ii) water photoelectrolysis, (iii) photoelectrocatalytic devices for the conversion of $CO_2$ to fuels, (iv) advanced Li batteries, (v) supercapacitors and (vi) fuel cells. In addition, other relevant devices in the field of energy (third-generation photovoltaic cells, nanostructured thermoelectric devices) are based on nanostructured materials closely related to those used in the cited electrodes.[1]

In all these electrodes, the common problem is how to control/optimize the mass and charge transport (i.e. electronic and ionic mobility), the electron-transfer kinetics at multiphase boundaries, and the modifications on the pro-

[a] Department of Industrial Chemistry and Engineering of Materials, University of Messina,
Salita Sperone 31, 98166 Messina, Italy
Fax: +39-090-391518
E-mail: centi@unime.it
perathon@unime.it

*Gabriele Centi is full professor of Industrial Chemistry (Univ. Messina, Italy). He was President of the European Federation of Catalysis Societies (EFCATS) and is President of the European Research Institute for Catalysis (ERIC), Coordinator of the Network of Excellence IDECAT and of the "Large Collaborative Project" NEXT-GTL. He is also Director of Section 2 (Energy and Environment) of INSTM and Scientific Coordinator of the Italian Technology Platform of Sustainable Chemistry. He is a Chairman of the Editorial Board of the Wiley-VCH journal ChemSusChem, and Chief Editor of the Book Series Studies in Surface Science and Catalysis published by Elsevier Science (Amsterdam). He is author of over 285 scientific publications (including over 20 reviews) and several communications in international conferences. He is author/editor of 8 books of catalysis and 8 special issues of international journals.*

*Siglinda Perathoner is associate professor of Industrial Chemistry (Univ. Messina, Italy). She is author of about 130 publications and several communications at international congresses, co-editor of 4 books and special issues of international journals of catalysis, author of various contributions to encyclopaedias on topics of catalysis. Furthermore, she is co-author of 12 reviews in international journals. She was coordinator of several EU projects in the area of catalysis for environmental protection and energy. Her present interests comprise the development of nanostructured catalysts for new processes with low environmental impact (both in the heterogeneous phase and under supercritical conditions), the development of catalytic membranes, the conversion of $CO_2$ with electrocatalytic devices, the development of nanostructured photoactive materials for fuel cells and the production and/or separation of $H_2$.*

  

cesses that occur upon application of a potential between the electrodes.

For example, in the electrodes of PEM (Polymer Electrolyte Membrane) fuel cells it is necessary to optimize (i) the three-phase contact between the proton-conducting medium, the electron-transporting carbon substrate and the gas phase, (ii) the rate of transport of protons, electrons and reactants ($H_2$ at the anode and $O_2$ at the cathode) and products ($H_2O$ at the cathode) and (iii) the surface processes at the electrocatalytic sites (i.e. Pt-based nanoparticles) as well as the changes in these processes, which occur upon charging the nanoparticles during electrochemical operations (application of a voltage or current between the electrodes).

In batteries, it is also necessary to coordinate mass transport, charge transport (electronic and ionic mobility) and electron-transfer kinetics in order to store or release energy. A poor charge-carrier mobility and electron transfer to adsorbates limit the efficiency of energy conversion in $TiO_2$-based materials for water photoelectrolysis, not only because the rate of charge recombination increases, but also because of surface quenching effects. Therefore, optimization of the performance requires the ability to control a complex reaction environment, where many kinetic aspects simultaneously concur in determining the performance.

Many of these controlling aspects are size-dependent, and thus the area of devices for energy conversion and storage has naturally dedicated great attention to prepare nanostructured materials. For example, traditional electrode materials for Li batteries are based on micrometre-sized materials, which have both mixed electron and ion transport (for $Li^+$), such as (i) layered metal oxides that have high redox potentials and act as positive electrodes and (ii) graphitic carbons capable of reversible uptake of Li at low potentials, which act as negative electrodes. The use of nanostructured solid-state materials allows, as a result of the intimate nanoscale contact, not only increasing the power density, but also enhancement of Li reversibility and thus cycle life.[22] In fact, the cycling ability of $Li^+$ ion transfer depends on the dimensional stability of the host material during insertion and deinsertion of $Li^+$ ions. Mechanical stress occurs during charge/discharge cycles, causing cracks and finally loss of performance.

These phenomena are reduced by decreasing the size to nanometre dimensions. Therefore, nanostructured materials for energy harvesting, conversion and storage do not show only an improvement of the performance with respect to micrometric-sized materials as a result of the increased surface-to-volume ratio, but also because of "true size effects" related to a change in material properties when going to nanometric size.[2,20,21]

## 2. The Role of Nanoarchitecture

Recently, it was recognized that not only the nanodimension would be relevant, but that the nanoarchitecture of these materials was also critical, for example in photoactive 1D[23] and 2D-type[24] $TiO_2$-based materials. Materials based on oriented nanostructured 2D films possess better properties in various key areas of energy technology, namely photovoltaics, batteries, supercapacitors and thermoelectrics.[1] On the other hand, 2D-type electrochemical cells are limited in the amount of energy that they can store or the amount of power that they can deliver. Multilayered nanoarchitecture[25] is a possible approach to solve this problem, or alternatively 3D architectures based on appropriate nanoscale building blocks.[17,26–28]

The concept of hierarchically organized materials is a useful approach to reach the above objectives. The development of a multilevel 3D organization based on a host macrostructure allows the right 3D organization necessary for a fast mass transport, for example. On this host macrostructure, a secondary guest micro- and/or nanoscale substructure is built in order to take advantage of the properties of nanometre-sized building blocks and micron- or submicron-sized assemblies.

Guo et al.[2,6] proposed for Li-ion batteries a hierarchical 3D mixed conducting network on both nanoscale and microscale levels in order to reduce the effective diffusion length to a few nanometres. The approach is to prepare a dense assembly of electroactive nanoparticles ($TiO_2$), leaving between them a mesoporous network in which electronic conductor nanoparticles ($RuO_2$) and the electrolyte are present to allow migration of both $Li^+$ and $e^-$. These nanoassemblies are put in a microenvironment formed by carbon black particles, which disperse the nanoassemblies and provide good electron conduction. The nanoassemblies allow low diffusion times, enhanced local conductivities and faster phase-transfer reaction, while the micronetwork formed by the nanoassemblies dispersed in the carbon black allows high absolute capacities.

Similarly, it is possible to synthesize by a polyol process vanadium oxide nanorods that self-assemble to form hollow microspheres showing high capacity and remarkable reversibility when used as cathode materials in Li-ion batteries.[29] In an electrode composed of nanoscopic particles, a higher surface area per volume is present with respect to an electrode composed of large particles. This mitigates the slow electrochemical kinetics related to solid-state diffusion of $Li^+$ ions during the discharge process and the reverse mechanism during the charge process [Equation (1)].

$$x\mathrm{Li}^+ + x\mathrm{e}^- + \mathrm{V_2O_5} \underset{\text{Charge}}{\overset{\text{Discharge}}{\rightleftharpoons}} \mathrm{Li}_x\mathrm{V_2O_5} \quad (1)$$

Sides and Martin[30] demonstrated that, by using a cathode composed of nanodispersed $V_2O_5$ nanofibres (diameter about 70 nm) that protrude from a current-collector surface (like the bristles of a brush) it is possible to obtain a dramatic increase in the low-temperature performance with respect to a similar electrode architecture based on larger $V_2O_5$ fibres (0.45 or 0.8 μm in diameter). The effect is not proportional to the surface area of $V_2O_5$ fibres and is larger than that expected from only a faster solid-state kinetics.

Sun et al.[31] have shown that highly ordered or defect-rich $V_2O_5$ nanorolls may be produced in controlled syn-

  

thetic conditions. The defect-rich nanorolls show enhanced electrochemical properties, due to a higher number of redox sites and increased interlayer accessibility of the alkali ions as a result of cracks and exfoliation. Therefore, upon decreasing the size of $V_2O_5$ fibres, not only does the exposed surface area change and the solid-state path for $Li^+$ diffusion decrease, but also different defective characteristics of the material can be produced. Although this aspect is often not considered, also because of the intrinsic difficulty of characterizing the presence, nature and amount of defects in nanomaterials, it plays a considerable role in determining the electrochemical properties.

It is known that defects are stabilized as the particle size decreases, although the nanoscale form also plays a role.[32,33] When the number of defects increases, however, the electronic conduction (bulk and surface conduction) of the oxide is affected.[34,35] In addition, out of the need to maintain structural integrity along a high series of discharge-charge processes, a large number of defects are negative. Therefore, it is necessary to combine highly accessible nanoscale architecture with a crystalline habit, but including localized defects that can enhance the redox and diffusion properties. At the same time, a proper nanoarchitecture would also be necessary to minimize the path of $Li^+$ diffusion in the electrolyte. Therefore, the performance of the electrode depends on the complex interdependence between (i) nanoparticle size, shape and characteristics, (ii) nanoarchitecture and hierarchical organization, and (iii) electronic and nanoionic properties of the material.

In order to solve this complex problem, it is useful to explore the use of hybrid materials. The most direct option is to develop hybrid nanostructured $V_2O_5$/carbon materials. Nanorods of several oxides ($V_2O_5$ and others), with diameters at 10–200 nm and lengths up to a few microns can be prepared by using carbon nanotubes (CNTs) as template.[36] A hybrid system can be thus simply prepared by avoiding to remove the CNT template. However, the $V_2O_5$ nanorod is inside the CNT, and thus accessibility by $Li^+$ ions is limited. Vanadium oxide may be instead deposited on the external surface of CNTs or carbon nanofibres (CNFs). Kim et al.[37] observed the formation of an amorphous and hydrous vanadium oxide ($V_2O_5 \cdot xH_2O$) thin film of approximately 6 nm thickness. This film shows a threefold higher specific Li-ion capacitance with respect to $V_2O_5 \cdot xH_2O$ prepared on a Pt plate substrate. Fang and Fang[38] also evidenced that $V_2O_5$ nanofilms uniformly distributed on N-doped carbon nanotubes exhibit significantly enhanced properties. Cross-sectional scanning electron microscope images show that CNTs provide a good support for uniform distribution of vanadium pentoxides.[39]

However, CNTs also induce the nucleation of 1D vanadium oxide nanostructures, and the nuclei grow into long, free-standing nanorods.[40] The vanadium oxide nanorods ($V_2O_x$-NRs) have an average length of 20 μm and diameter of 5–15 nm (Figure 1a). The CNTs thus induce the nucleation of oxide nanorods stabilized by the interaction with carbon, because $V_2O_x$-NRs are difficult to synthesize in the absence of a template. The CNTs also provide good electronic contact for a fast electron transport and may be grown over a hosting macrosubstrate, for example carbon cloth (CC) to realize a nanostructured 3D electrode: $V_2O_x$-NR/CNT/CC. The carbon cloth macrofibres have a diameter in the micron range, with respect to the 50–100 nm range for CNTs, which were grown over the CC by the chemical vapour deposition (CVD) method[41,42] (see Figure 2). The CNT/CC thus acts as substrate for an optimal 3D hierarchically organized structure and an efficient electron collection, provides a good dispersion of vanadium oxide, and also allows the growth of specific 1D-type nanomorphologies under the proper conditions of synthesis.

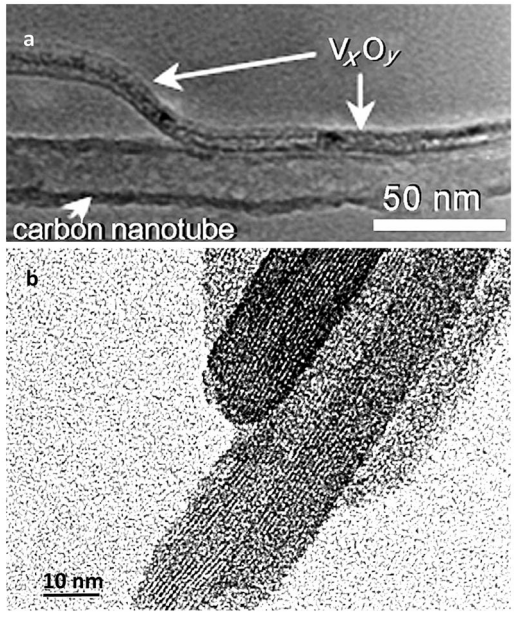


Figure 1. (a) Nucleation and peeling of a vanadium oxide nanorod from the surface of a CNT. (b) High-resolution transmission electron microscopy (HRTEM) image of vanadium oxide nanorods. Adapted from ref.[40] There is a design problem in finding the optimal compromise between nanosize, nanoarchitecture, robustness and stability, and performance per unit weight or volume, together with a cost-effective and scalable method of producing the electrode.

In fact, 1D-type nanostructures show enhanced surface area with respect to the equivalent 3D-type nanostructure. For example, for a nanorod of 10 nm diameter and 100 nm length, a spherical nanoparticle would have a diameter of about 12.3 nm for the same total volume and mass of vanadium oxide. The ratio of the two surface areas is about 1.8. This ratio increases for longer nanorods and largely increases in passing from a rod to a tube morphology.

The HRTEM image of $V_2O_x$-NR (Figure 1b) shows a well-ordered crystalline structure with an average layer distance of about 0.7 nm.[40] However, electron energy loss spectra (EELS) indicate that the nanorods contain both $V^{5+}$ and $V^{4+}$, and XRD patterns show the presence of a $V_2O_x \cdot xH_2O$-like phase instead that of $V_2O_5$ crystallites.[40] This is consistent with the results of Fang et al.[38,39] show-

  

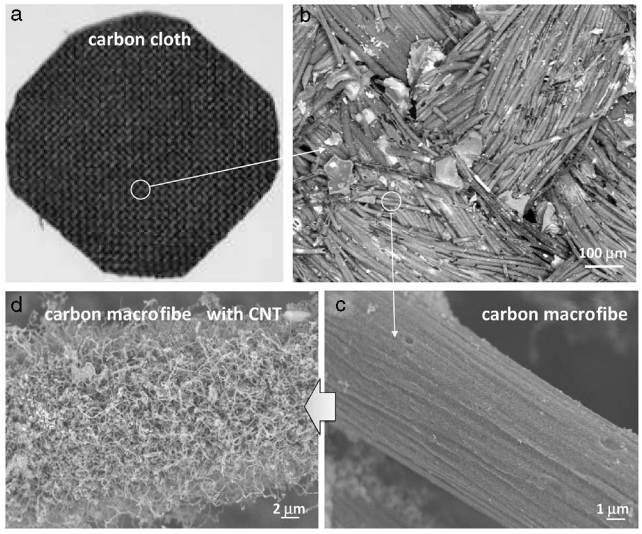


Figure 2. (a) Image of a $2 \times 2$ cm piece of carbon cloth (CC). (b,c) Scanning electron micrographs (SEM) of the CC at different magnifications. (d) SEM image of a carbon macrofibre after growing CNTs by chemical vapour deposition. Adapted from ref.[41,42]

ing the presence of hydrous vanadium oxide supported on CNTs. Therefore, supporting vanadium oxide on CNTs induces a better dispersion and a change in the morphology of the oxide with a modification of its specific characteristics. The presence of $V^{4+}$ even after calcination suggests that oxygen vacancies are stabilized in the $V_2O_x$-NR, favouring the reactivity with $Li^+$ ions. This is different from the case of conventional vanadium oxide obtained with the same method ($NH_4VO_3$ hydrolysis) but in the absence of carbon nanotubes.

This concept of nanoarchitecture of Li-ion battery electrodes was extended recently by preparing carbon tube-in-tube materials (CTITs). CTITs are built by a narrower inner tube inside an outer tube. They can be assembled by a wet chemical reorganization of carbonaceous impurities around and inside pristine nanotubes.[43] First, the graphitic nanoparticles are disintegrated into small fragments by an $HNO_3$-based oxidation at defective sites. Secondly, the small graphene fragments are reintegrated around or inside pristine nanotubes to assemble CTITs by acid-catalyzed esterification linkages between the carboxyl and hydroxy groups. Figure 3 shows microscope images of CTITs and schematically outlines the mechanism of formation of the second tubes, by wet reorganization of the graphene fragments, on the outer or inner sides of pristine carbon nanotubes. The combination of the two mechanisms leads to the synthesis of triple tubular nanostructures.

An alternative procedure to prepare *nano-in-nano* carbon structures is based on the selective deposition of an active metal (Co nanoparticles with an average size of 6.6 nm) on the inner walls of CNTs (inner diameter in the 20–80 nm range), which was followed by the growth of CNFs by means of catalytic chemical vapour deposition (with a 1:1:2 mixture of $C_2H_4/H_2$/He as feed).[44]

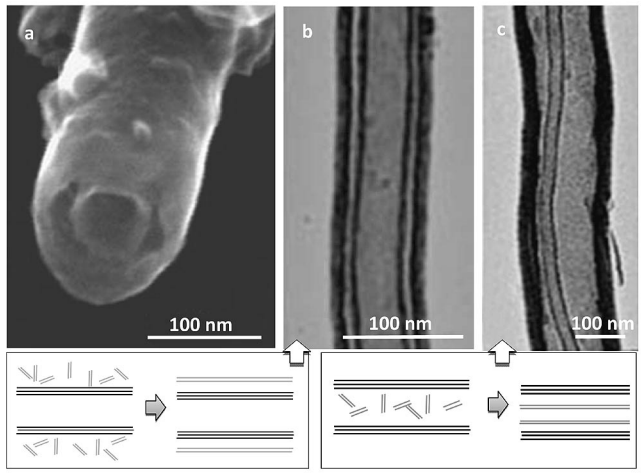


Figure 3. (a) SEM image of the end of a typical tube-in-tube assembly confirming the encasing tubular structure. (b) TEM images of CTITs with relatively small and uniform interval spaces, which exhibit similar morphologies between the inner and outer tube moieties. Such tubes are likely to be produced from the assembly of graphitic fragments around the pristine tubes. (c) TEM images of CTITs with large and highly irregular interval spaces and very thin inner tubes (about 30 nm). Such CTITs are formed via the assembly of graphitic fragments within the pristine tubes. The schemes below the images describe the formation of the tube structures shown in (b) and (c). Adapted from ref.[43]

The concept is shown in Figure 4, which also reports in the insets SEM images of the pristine CNTs and as-prepared CNFs@CNTs (carbon nanofibres included in the carbon nanotubes). High-resolution SEM and transmission electron microscopy (TEM) images also evidence that as-synthesized CNTs are open at the end and have approximately 100 nm outer diameter and 0.2 mm length. Tilting the TEM specimen confirmed the good confinement of CNFs within the CNTs. The specific surface area increased from 82 $m^2/g$ to 347 $m^2/g$ after inclusion of CNFs in the CNTs, which suggests a greatly improved utilization of space inside the hollow channels of the CNTs.

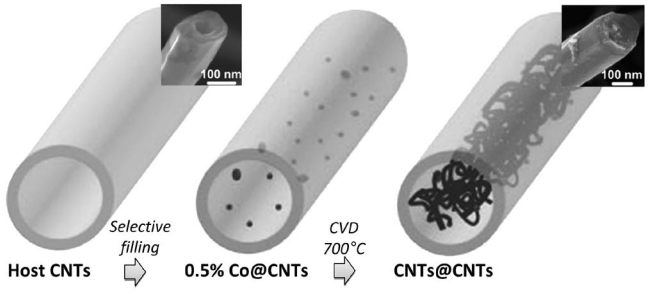


Figure 4. Scheme of the synthesis route to carbon-nanotube-encapsulated carbon nanofibres (CNFs@CNTs). In the insets, SEM images of the pristine CNTs and as-prepared CNFs@CNTs. Adapted from ref.[44]

By using these carbon tube-in-tubes as a nanoreactor and an efficient mixed-conducting network, a new design was proposed for nanostructured electrodes for high-per-

  

formance Li batteries.[45] The concept is based on the use of hierarchical mixed-conducting networks, i.e. networks that can conduct both ions and electrons.

This concept was realized by the synthesis of mesoporous $TiO_2$:$RuO_2$ and C-$LiFePO_4$:$RuO_2$ nanocomposite electrodes, which show high rate capabilities when used as the anode and cathode materials for lithium batteries.[46,47] There are two keys to the success of this procedure: First, the preparation of mesopores, which render the diffusion of electrolyte into the bulk of the electrode material facile and hence provide fast transport channels for the conductive ions (e.g., solvated $Li^+$ ions). Second, the coating of pore channels by a good electronic conductor (the oxide $RuO_2$) that enables a fast electronic transport pathway.

CTITs or CNFs@CNTs, in combination with nanosized $V_2O_5$, would constitute a cost-effective alternative to the above-mentioned $TiO_2$:$RuO_2$, because of the high electronic conductivity of carbon, good lithium permeation and electrochemical stability. The proposed nanoarchitectured electrode is composed of an efficient mixed-conducting network (Figure 5), in which the CTIT serves as an "electronic wire" to provide the electrons to the active materials, and the specifically designed tube diameter of the CTIT allows easy electrolyte access.[45] Such a nanostructure provides both electronic and lithium-ion pathways, which are essential for a high-rate rechargeable lithium battery. The kinetics of Li insertion/extraction and the Li storage performance are improved over those of conventional materials for two main reasons: The first is the close electrical contact between the phases at the nanoscale level along the wall of the CTIT. The second is the easy accessibility of the material to the electrolyte.

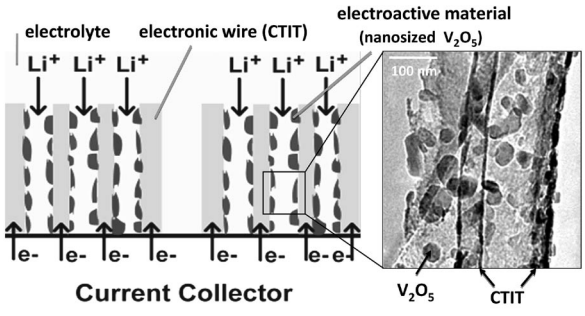


Figure 5. Design for an efficient mixed-conducting network for Li-ion batteries based on CTIT and nanosized $V_2O_5$. The inset shows a TEM image of the $V_2O_5$/CTIT nanocomposites showing that most of the $V_2O_5$ nanoparticles are encapsulated within CTITs. Adapted from ref.[45]

The use of CTITs or CNFs@CNTs provides a more effective nanoenvironment with respect to CNT, increasing the effectiveness of the dispersion and amount per volume of the oxide and thus the storage capacity of the battery. The CTIT also acts as a nanoreactor for the synthesis of nanomaterials, by exploiting its multiple channels and the possibility of confining reagents within them.[45] Cyclic voltammetry tests of the Li charge/discharge behaviour of $V_2O_5$/CTIT nanocomposites confirm the fast kinetics and the retention of capacity upon cycling.[45]

A nanocomposite of mesoporous $TiO_2$ and single-walled carbon nanotubes showed a high capacity, even at high charging-discharging rates, due to the presence of nanochannels for both ion and electron transport.[48]

Brookite-type $TiO_2$/carbon nanocomposite electrodes for application to Li ion batteries were tested by Lee et al.[49] CNTs loaded with Ag and $TiO_2$ nanoparticles also show high cycling stability and a high reversible capacity after several cycles.[50] Ag addition increases the electronic conductivity of the composites and allows convenient transfer of Li ions in the composite structure. The $TiO_2$/CNT nanocomposite could be prepared by a self-assembling method.[51]

The alternative nanodesign for Li-ion batteries is to directly nanostructure an oxide such as $TiO_2$, which can act both as the electroactive element for the $Li^+$ charge/discharge process and as the electroconductive material. This would clearly simplify the process of production and reduce the costs. $TiO_2$ is an attractive anode material for Li-ion batteries because of its high capacity, high mechanical stability during Li intercalation/deintercalation process, limited side reactions with the electrolyte, low cost and environmental friendliness.[52]

$TiO_2$ (Brookite), obtained from titanate nanosheets, shows excellent properties in the charging/discharging capacity for Li ion intercalation.[53] Nanosized anatase $TiO_2$ particles[54] and nanorods,[55] as well as rutile $TiO_2$ nanorods,[56] were also found to have interesting performance as electrodes for Li-ion batteries. For titania, it was observed that the decrease in particle size from the micron to the nano range influences the phase morphology and Li-ion mobility.[57] Many other authors have investigated titania as the material for preparing Li-ion battery electrodes.[58–60] However, the issue is how to combine a suitable nanostructure with a small particle size and an efficient mixed-conducting network.

Various methods were developed for preparing $TiO_2$ nanoparticles, nanorods, whiskers, nanowires, nanotubes and nanotube arrays, as well as mesoporous $TiO_2$ films[23,24,61–64] or titanates and related nanostructures.[65,66] Four general approaches (wet methods such as template assisted, anodic oxidation, alkaline hydrothermal and dry methods such as CVD or related methods) for the preparation of nanostructured titanate and $TiO_2$ can be used. However, the following cases must be differentiated: (i) a random assembling of quasi 1D nanostructures (nanorods, nanowires, nanotubes, etc.), (ii) a film characterized by an ordered nanostructure (for example dense and well-aligned $TiO_2$ nanorod or nanotube arrays), (iii) a thin membrane characterized by aligned nanoholes and (iv) an assembly of nanoparticles, even with a relatively narrow size distribution. The properties of these materials are highly dependent on the nanostructure and nanoarchitecture, as well as on the crystalline phase, the presence of impurities and defects, etc.

In general, there is an increasing interest in the use of inorganic nanotubes and nanowires in Li storage. In addition to $TiO_2$, various other inorganic 1D-type materials

  

($MoS_2$, $WS_2$, $TiS_2$, $MnO_2$, $V_2O_5$, $SnO_2$, etc.) have been investigated, as reviewed by Cheng and Chen.[67] It was observed that 1D inorganic nanostructures like tubes and wires exhibit superior electrochemical characteristics, because of the combined advantages of small size and 1D morphology.

Zhou et al.[68] were among the first to investigate lithium insertion into $TiO_2$ nanotubes (TiNTs) prepared by the hydrothermal process. This preparation method is based on the morphological reorganization of $TiO_2$ nanoparticles occurring in strong alkaline medium under hydrothermal conditions (temperatures of around 130–140 °C). TEM tests showed that uniform straight hollow tubes with diameters of approximately 8 nm and lengths greater than 300 nm were formed, while XRD measurements indicated that the crystalline phase of the nanotubes is anatase $TiO_2$. Cyclic voltammetry and galvanostatic charging and discharging tests showed that Li-ion intercalation/deintercalation occurred reversibly in the $TiO_2$ nanotube electrode and that a high capacity was obtained.

The hydrothermal method produces typically low-diameter tubes. For example, Khan et al.[69] observed that titania nanotubes produced by the hydrothermal method show a multiwall anatase phase with an average outer diameter of 8 nm and an inner diameter of 5 nm and grow along the [001] direction to lengths of 500–700 nm with an interlayer fringe distance of about 0.78 nm. When these nanotubes are deposited on a surface to produce a thin film (for example, by dispersion in a solvent, which is then evaporated), a random orientation of TiNTs occurs in which several of them are in poor electrical contact with the conductive substrate. Therefore, their performance as electrode is not optimal. However, a nanostructured film characterized by an array of oriented TiNTs can be formed on a Ti substrate seeded with $TiO_2$ nanoparticles, which is then treated hydrothermally (NaOH solution, 150 °C, reaction time: 5–20 h).[70] SEM and TEM images suggested that a folding mechanism of sheet-like structures was involved in the formation of the nanotubes.

Figure 6 shows a SEM image of the arrays of oriented TiNTs prepared by hydrothermal treatment at 150 °C of the Ti substrate seeded with $TiO_2$ nanoparticles. In the inset, a high-resolution TEM image of the apical part of one of the nanotubes is shown. It may be observed that the inner diameter of TiNTs is about 3–4 nm (their length is up to 10 μm), but the film is not very dense. The average distance between the TiNTs is 10 to 20 times their external diameter. Although these parameters may probably be optimized by a proper seeding procedure and hydrothermal treatment, the synthesis procedure does not seem to be optimal for preparing electrodes for Li-ion batteries. Good contact with the Ti conductive substrate, however, could be observed.

An alternative method to produce a dense array of $TiO_2$ nanotubes is based on an electrochemically induced self-organization mechanism, which occurs during a controlled anodic oxidation of a titanium substrate.[24,71–74] The mechanism is essentially based on the anodic growth of an oxide layer on the Ti metal surface, the simultaneous chemical dissolution of the oxide in the presence of fluoride ions (or other complexing agents), and the field-induced self-organization to form the nanotubes.

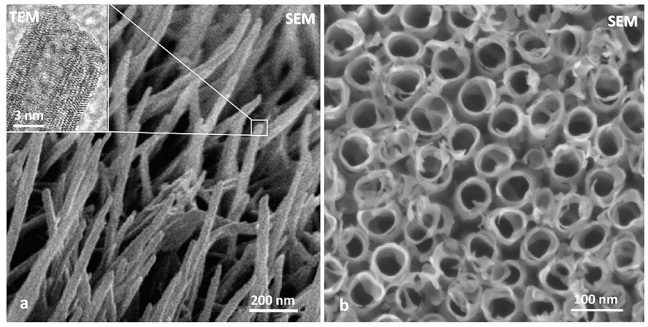


Figure 6. (a) SEM images of large arrays of oriented $TiO_2$-based nanotubes prepared hydrothermally at 150 °C on a Ti substrate seeded with $TiO_2$ nanoparticles. In the inset, high-resolution TEM image of the apical part of a nanotube. Adapted from ref.[70] (b) Field-emission SEM image of an array of $TiO_2$ nanocoils formed by anodic oxidation of Ti foil at 15 V. Adapted from ref.[74]

The first stage is the anodic growth of a compact oxide on the metal surface according to reaction (2).

$$Ti + 2H_2O \rightarrow TiO_2 + 4H^+ + 4e^- \quad (2)$$

In the presence of fluoride ions, chemical dissolution of the oxide as soluble fluoride complexes, as shown in Equation (3), competes with reaction (2).

$$TiO_2 + 6F^- \rightarrow [TiF_6]^{2-} \quad (3)$$

Further oxide growth is controlled by field-aided ion transport ($O^{2-}$ and $Ti^{4+}$ ions) through the growing oxide. As the system is under a constant applied voltage, the field within the oxide is progressively reduced by the increasing oxide thickness. The process is thus self-limiting.

The decreasing field strength leads to an exponential current decay and thus to the growth of a compact oxide layer with a finite thickness. If $Ti^{4+}$ ions arriving at the oxide/electrolyte interface are not "made soluble" by complexation, a hydroxide layer will precipitate in most electrolytes. This layer is typically loose and porous, and it thus does not contribute to field effects, but exerts, to a certain extent, diffusion-retarding effects.

In the presence of $F^-$, the situation becomes more complex. This is mainly due to two effects of the fluoride ion: (i) its ability to form water-soluble complexes according to reaction (3) and (ii) its small ionic radius, making it suitable to enter the growing $TiO_2$ lattice and to be transported through the oxide by the applied field (thus competing with $O^{2-}$ transport). The complex formation ability leads to a permanent chemical attack (dissolution) of formed $TiO_2$ and prevents the precipitation of $Ti(OH)_xO_y$, as $Ti^{4+}$ ions arriving at the oxide/solution interface can be solvatized to $[TiF_6]^{2-}$ before reacting and precipitate as a $Ti(OH)_xO_y$ layer. Figure 7 reports a simplified scheme of the evolution of the $TiO_2$ morphology during anodic oxidation of a Ti foil in the presence of fluoride ions.

  

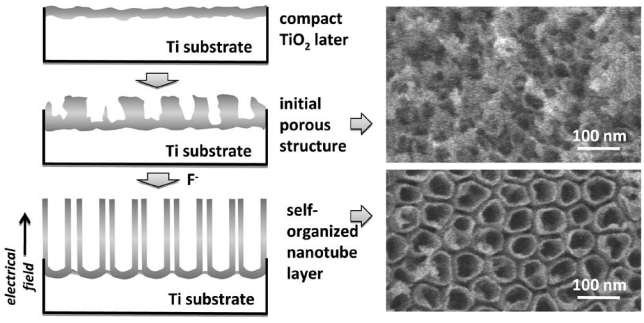


Figure 7. Evolution of the $TiO_2$ morphology during anodic oxidation of a Ti foil in the presence of fluoride ions.

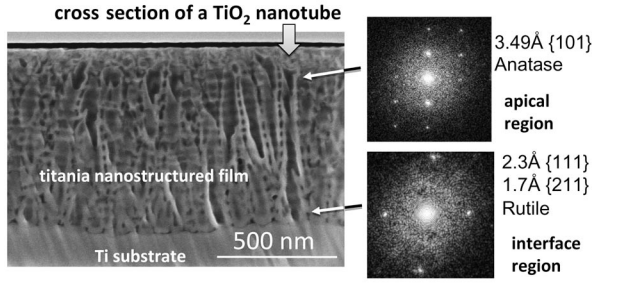


Figure 8. Left: SEM image of the cross section of a $TiO_2$ nanostructured film produced by anodic oxidation of a Ti substrate. Right: electron diffraction images (obtained by a high-resolution TEM apparatus) of selected areas at the interface region between the oxide film and the Ti substrate and at the apical region of the $TiO_2$ nanotubes.

By changing the parameters (voltage, fluoride ion concentration, solvent, temperature, etc.), a variety of different nanostructured titania films could be produced, such as ordered arrays of nanotubes, -coils or -pillars, as well as nanosponges and random assemblies of very small nanoparticles.[75]

The exact mechanism of formation of these different nanostructures is still not completely clear,[71] but it derives from a combination of field-induced self-organization of the small $Ti(OH)_xO_y$ layer produced according to the mechanism discussed above and diffusion gradients. Note that, as a result of the presence of an initial porous structure, the electrical field is not spatially homogeneous over the electrolyte surface.

The nanotubes formed after the anodization process are amorphous, but crystallization occurs by annealing at temperatures above 300 °C. However, the morphology and shape of the nanotubes is fully retained during annealing, at least below about 650 °C. Anatase $TiO_2$ is observed by XRD after annealing in the 300–450 °C region, while at higher temperatures the presence of rutile $TiO_2$ could be also observed.

The structure of the nanotubes or other similar 1D-type nanostructures, however, is not isotropic. Figure 8 shows that, after annealing at temperatures below 450 °C, where XRD patterns do not evidence the presence of the rutile phase, the presence of this phase in the interface region between the Ti substrate and the $TiO_2$ nanotube (i.e. at the bottom of the nanotube) could be evidenced by electron diffraction in high-resolution TEM images.[76] In addition, electron energy loss spectra (EELS) show that the interface region is characterized by the presence of oxygen vacancies, i.e. of a $TiO_{2-x}$ phase. As discussed before, this aspect is relevant, as it favours a faster redox mechanism of Li intercalation/deintercalation. The presence of an anisotropic phase could also be relevant for behaviour as a Li-ion cathode, but it is particularly important for behaviour as a photoanode, as discussed later.

Schmuki et al.[77] first reported an investigation of Li insertion into highly ordered nanotubular layers of $TiO_2$. The nanotubes were formed by anodization of Ti in a $H_3PO_4$ (1 M) + NaOH (1 M) + HF (0.5 wt.-%) electrolyte at 20 V. This leads to nanotubular layers with a thickness of about 1 μm, an individual tube diameter of about 100 nm and a tube wall thickness of about 10 nm. The cathodic behaviour of tubes was studied in the as-formed amorphous phase and after being annealed to anatase. The latter show enhanced uptake for $Li^+$ and a very strong and reversible electrochromic effect.

Liu et al.[78] investigated anatase $TiO_2$ nanotube arrays prepared by anodization and annealed at 300°, 400° and 500 °C in $N_2$. Li-ion intercalation measurements revealed that annealing in $N_2$ resulted in an enhanced Li-ion insertion capacity and improved cyclic stability. $TiO_2$ nanotube arrays annealed at 300 °C exhibited the best Li-ion intercalation ability with an initial discharge capacity of 240 mA h/g at a high current density of 320 mA/g. The good discharge capacity at a high charge/discharge rate can be attributed to the large surface area of the nanotube arrays and a short facile diffusion path for Li-ion intercalation as well as improved electrical conductivity. As the annealing temperature was increased, the discharge capacity decreased, but the cyclic stability improved. $TiO_2$ nanotube arrays annealed at 400 °C had an initial discharge capacity of 163 mA h/g and retained 145 mA h/g at the 50th cycle.

By increasing the annealing temperature, i.e. the degree of crystallization, the number of defects and strains, as well as the surface area, is decreased. Both of these effects contribute to a decrease in the discharge capacity, although this is partially compensated by a better electrical conductivity and stability during a series of charge/discharge cycles.

The inner diameter of the titania nanotubes studied by Liu et al.[78] was approximately 100 nm (wall thickness about 10 nm) before calcination, while their film thickness was about 1.1–1.2 μm. Their surface area was in the 50–80 $m^2/g$ range. If one compares these results with those obtained by using anatase $TiO_2$ nanotubes produced by the hydrothermal method (diameter about 10 nm and lengths of 200–400 nm),[79] it is possible to see that the discharge capacity of $TiO_2$ arrays produced by anodic oxidation is about 30% lower than that of $TiO_2$ nanotubes produced by the hydrothermal method. The reason is that the density of nanotube array packing and the surface area increase when the $TiO_2$ nanotube diameter is reduced. In addition, a length of over one micron (film thickness) would certainly create diffusion resistance for the electrolyte.

  

Ortiz et al.[80] reported recently the discharge/charge properties and cycling performance characteristics of amorphous and crystalline titania nanotube arrays prepared by anodization. The nanotube characteristics are quite close to those studied by Liu et al.[78] A maximal areal capacity of 77 μA h/cm$^2$ and a good capacity retention up to 90% over 50 cycles were observed. The areal capacity decreases for fast kinetics, confirming the previous observation of the presence of diffusion limitations.

Therefore, the performance and stability of a Li-ion battery electrode based on an ordered array of titania nanotubes should be further improved by an optimized design of the nanostructure, even if the advantage of a simple preparation and easy implementation in multistacks should be accepted. A more dense $TiO_2$ nanotube array (i.e. smaller diameter, probably in the 15–30 nm range), thinner films (below 500 nm) and structures with regular, straight channels should be prepared. This is possible by controlling the voltage, [HF] and temperature during anodization.[74,81,82] On the other hand, stability and electronic conductivity should be improved. Stability is related to the reversibility of Li insertion, which also depends on the characteristics of the titania nanotubes, as well as on annealing, as observed above. Figure 9 shows that the voltage applied during the anodization process influences the packing density, the average diameter of nanotubes and the wall thickness.

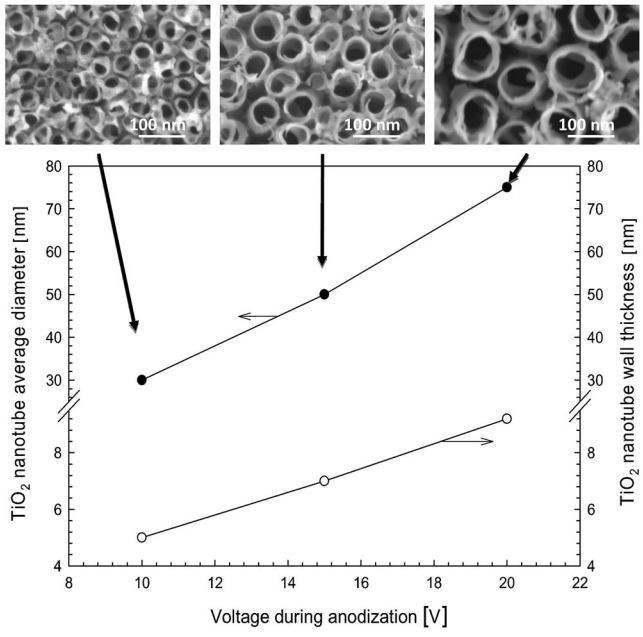


Figure 9. Relationship between voltage during anodization of Ti films and average nanotube diameter and wall thickness. Top: field-emission SEM images of the different samples. Adapted from ref.[74]

A closer inspection of the SEM images (see also Figure 6b) shows that the nanotube structure produced by this specific procedure[74] differs from the ideal model of nanotubes schematically shown in Figure 7. In fact the nanostructure may be better described as a nanocoil, i.e. a rolled thin ribbon. This nanostructure is preserved upon annealing and appears rather interesting for Li-ion batteries, because the specific thickness is very small (drastically reducing the solid-state diffusion to few nm only), and the nanostructure may easily adapt to volume changes after lithiation, thus increasing reversibility.

The electronic properties may be further enhanced by doping. Decoration of $TiO_2$ nanotubes by Sn nanoparticles of an approximate size of 10 nm improves the retention of reversible capacity on cycling for Li intercalation.[83] The deposition of Ag nanoparticles on $TiO_2$ nanotubes significantly improves the electronic conductivity, charge-discharge capacity and cycle stability of the $TiO_2$ nanotubes,[84] because Ag decreases the polarization of the anode.[85] Therefore, doping constitutes a valuable opportunity, although it has still not been investigated in detail, to further promote the properties of $TiO_2$ nanotube array electrodes.

There is a large interest in literature on the development of nanosized transition-metal oxides as anodes for Li-ion batteries.[86–90] Nanostructuring leads to increased reaction areas, shortened $Li^+$ diffusion and enhanced solubility/capacity. In addition to titanites and titanium oxides,[90–94] other metal oxides have been demonstrated to allow to prepare stable and high-capacity anodes for Li-ion batteries.

Meduri et al.[94] reported the use of Sn nanoclusters supported on $SnO_2$ nanowires as anodes for Li-ion batteries. They observed a capacity greater than 800 mA h/g over one hundred cycles with a low capacity fading of less than 1% per cycle. The good performance was attributed to the easy volume expansion during Li alloying and reverse de-alloying in this nanostructure. Chang et al.[95] investigated instead the behaviour of nanocomposite $SnO_2$/Sn deposited uniformly on a graphite surface, while Liang et al.[96] investigated the behaviour of tin oxide doped with $SiO_2$. Due to the different experimentation, a direct comparison is not possible, but in general, all these tin-oxide-based anodes for Li-ion batteries show interesting performance and stability. Other nanostructured metal oxide anodes investigated recently include nickel oxide nanowires (diameter about 25 nm),[97] nanosized $MoO_2$,[98] iron oxide nanoflakes[99] or nanotubes,[100] manganese oxide nanofibres,[101] $Cu_2O$ nanorods[102] and various mixed oxide nanosized materials, such as $ZnFe_2O_4$[103] with spinel structure and metal-doped $Li_2Ti_3O_7$[104] with ramsdellite structure. Interesting properties are also shown by oxyfluorides such as $TiOF_2$ and $NbO_2F$.[105]

It should be noted that the data do not provide a full comparison, in terms of performance and stability, to determine the preferable class of materials. In addition, often a clear rationale to investigate new materials is missing. Nevertheless, it is evident that there is very active research on the development of metal-oxide-type anodes for Li-ion batteries. It is also well demonstrated that the nanostructure of these materials is the conditioning factor to obtain high performance. The Ti-based materials appear to be preferable, in particular with regard to stability, robustness and easy fabrication, but tin oxide materials also demonstrate good characteristics.

  

The examples discussed in this section, although mainly focused on some aspects of the development of electrodes for Li-ion batteries, have shown the great potential of the proper design of the nanostructure and -architecture of electrodes. However, still the largest part of the studies is not based on an in-depth understanding of the complex physicochemical phenomena occurring at the nanoscale. Most of the aspects discussed here are of general relevance for the development of nanostructured electrodes for other applications, such as fuel cells, photoanodes and electrodes for $CO_2$ conversion. These other applications have their specificity, as will be discussed later.

In all cases, however, there is the need to combine enhanced processes at a nanoscale level to a macroscale structure, which allows high capacity, efficient mass transport and multiphase contact. In other words, the issue is how to realize an efficient hierarchically organized structure that should also meet other critical requirements, such as stability and robustness, cost-effectiveness and easy scale-up.

## 3. Synthesis of Nanoarchitectured Electrodes

There are many advanced methods to prepare tailored hierarchically organized structures for electrodes, even if a detailed analysis of the methods of synthesis to produce inorganic micro-/nanostructured materials is out of the scope of this survey. Various reviews have been published on this topic recently,[106–111] and we thus recall here only selected aspects.

Ordered metal nanostructures with hierarchical porosity (macropores in combination with micro- or mesopores) can be prepared by using colloidal crystals (or artificial opals), i.e. ordered arrays of silica or polymer microspheres, as templates on which the metal particles can be deposited. An ordered metal nanostructure[89] is then obtained by careful removal of the template material. The extension of the concept of template synthesis for tailored nanomaterial properties is the synthesis of replica mesostructures by nanocasting.[112]

Nanocasting by using highly ordered mesoporous silica as a template has brought forward incredible possibilities in the preparation of novel mesostructured materials and has led to a great number of ordered nanowire arrays with:
(a) small diameters (<10 nm);
(b) large surface areas (up to 2500 $m^2/g$) and uniform mesopores (1.5–10 nm);
(c) tunable 2D or 3D mesostructures;
(d) controlled morphology, such as spheres, rods, films and monoliths;
(e) different components including carbon, metals, metal oxides and metal sulfides.

The method has been initially used in the preparation of ordered mesoporous carbon materials.[113–117] Recent breakthroughs in the preparation of porous materials allowed to develop mesoporous carbon materials with extremely high surface areas and ordered mesostructures. Current synthesis methods can be categorized as either hard-template or soft-template methods, but the synthesis essentially involves infiltration of the C precursor in the template pores, its carbonization and subsequent template removal. Consecutive surface functionalization of the carbon materials obtained, for a further optimization of their characteristics, is possible. The carbon replica material can then also act as the template for other replica materials.

The nanocasting method can be used for the preparation of a variety of mesostructured and mesoporous materials,[118] including mesostructured metal[119] and semiconductor nanowires.[120]

Although powerful, the nanocasting method has clear limits in terms of cost and scale-up. The alternative approach is based on the synthesis of small-size particle units by using the various available physicochemical methods, such colloidal,[121] sol–gel[122] and micelle methods,[123] as well as other wet[124,125] or gas-phase[126] procedures. These nanounits may be then organized in 2D and 3D superstructures by self- or directed-assembling, seeded or field-induced growth, epitaxial growth or other nanostructuring procedures.[127–132]

The main limit of self-assembling is often the difficulty in tailoring the proper nanoarchitecture and avoiding a fractal-type growth. Some electrochemical methods, such as the anodic oxidation discussed in the previous section, fall within this category of self-assembling methods. The electrical field created at the interface between the electrode and electrolyte is a powerful factor for the orientation of nanostructure growth, as shown for titania electrodes. However, the reaction mechanisms and the factors controlling the formation of a specific nanostructure still has to be better understood.

The third general class of synthesis methodology for the development of tailored 3D nanoarchitectures is based on physical or physicochemical deposition methods. Layer-by-layer (LbL) deposition is a procedure often used for preparation of electrodes.[133–135] It is based initially on the electrostatic binding of a charged polymer to an oppositely charged surface. Multiple polymer layers are subsequently assembled by alternately immersing the substrate in positively and negatively charged polymeric solutions. The charge neutrality within a layer is maintained by a nonpolymeric counterion. It is possible to produce a stacked structure of well-controlled thickness, but the realization of porous 3D architectures is difficult. LbL assembly is a simple, versatile and relatively inexpensive approach by which nanocomponents of different groups can be combined to coat both macroscopically flat and nonplanar (e.g., colloidal core-shell particles) surfaces.[136] LbL can be used to combine a wide variety of species – including nanoparticles (NPs), nanosheets and nanowires (NWs) – with polymers, thus merging the properties of each type of material.

Atomic layer deposition (or epitaxy) is instead based on the deposition of a metal oxide precursor by using typically an organometallic complex to form a deposited monolayer, which is then converted by reaction with a second gas-phase reactant.[137] Multiple layers can be produced by repeating the cycle. Also this technique has been often used to modify

  

electrode surfaces, such as carbons,[138] anodic alumina membranes[139] and other substrates.[17] Metals, metal oxide or metal nitride thin films could be prepared.

These methods, as well as other methodologies that belong to this general class of thin film growth such as CVD, molecular-layer or pulsed-laser deposition, magnetron sputtering, etc.,[140–142] are suitable to prepare thin films, sometimes also nanostructured, or for coating a 3D structure with a thin layer. However, they may not be well-adapted for preparing ad hoc nanostructures. An additional issue is the scalability for preparing larger homogeneous samples.

Therefore, many synthetic methods are available for the preparation of nanoarchitectured electrodes and hierarchically organized materials for energy storage and conversion, but the cost-effectiveness of the preparation often receives little consideration. In other words, few studies evaluate whether the additional cost of synthesis with respect to conventional materials is worth for the additional enhancement of performance. Care is always necessary in considering the synthesis costs. The industrialization of a synthesis procedure may decrease largely the cost of production (by more than two orders of magnitude). However, a major issue is the reproducibility of the properties, when nanomaterials are produced on a larger scale. Carbon nanotubes show large deviation in their properties from batch to batch as well as within the batch itself. This is not critical when used for polymer composites, for example, but is an issue in electrode applications. Finally, robustness of the materials is a further aspect to consider in preparing nanostructured electrodes.

## 4. Nanoparticles vs. Nanostructures

Previous sections have shown that a wide variety of nanostructures with different morphology, size and composition have been investigated as electrode and related devices, but often their physical and electrochemical properties have not been fully understood, notwithstanding the relevant theoretical progress in the area.[143]

A key question in relation to the topic of this microreview regards the exact role of the nanoarchitecture in physical electrochemical processes. Are these processes at the nanoscale level influenced by the architecture of the material? We have already evidenced that the defective properties of the materials, for example, could be different in nanoparticles or nanorods and similar for the electronic transport properties. However, does an electrolyte confined within a nanotube have the same properties as an electrolyte surrounding nanoparticles? This is one of the questions raised in considering nanoparticles vs. nanostructures. Bisquert,[143] in his perspective paper, discussed some of these aspects in relation particularly to dye-sensitized solar cells (DSCs) based on nanocrystalline $TiO_2$. However, we should state the need for more extensive studies in this area on all types of electrodes in order to put on a more solid basis the design of nanostructured electrodes, which are mainly based on phenomenological studies today.

Very small crystals (below 5–10 nm) behave as quantum dots. In these crystals, the electron wave functions are strongly confined, i.e. the electron energy levels are discrete, and their separation is determined by the crystal size. Larger nanocrystals, in the range 10–50 nm, do not show the electron confinement effect, but are important for many applications, because they allow electrochemical gating (ECG), i.e., an increase in electronic density compensated by ionic density at the surface.

ECG is the ability to change the resistivity of a semiconductor nanoparticle (or of a carbon nanotube) by many orders of magnitude by applying a voltage between the material and a reference electrode in an electrolyte. The effect is related to the effect of the chemical species on the surface in samples having a large surface-to-volume ratio. The Fermi energy of the nanoparticle or nanotube can be changed, as ions from the solution accumulate on the surface and act as a close-spaced gate.

ECG is an important aspect in determining the properties of nanostructured electrodes and DSC devices. Examples of metal oxides used in DSCs are $TiO_2$, ZnO and $SnO_2$.[144,145] These nanocrystals are also the building blocks for the preparation of larger architectures.[146]

ECG is a known method to tune and monitor the (opto)-electronic properties of functional materials.[147] Electrochemical interfaces usually consist of a solid-phase electron conductor in contact with an ionic solution. In practice, the solid can be placed as working electrode in a conventional three-electrode electrochemical cell; its electrochemical potential is controlled by applying a voltage ($V$) with respect to a reference electrode (Figure 10). A change in the potential of the working electrode can lead to a change in the electrostatic potential drop over the electrochemical double layer, while the Fermi level in the solid remains unchanged with respect to the energy levels of the solid. Alternatively, a potential drop can develop across the interfacial part of the solid inducing a change in the Fermi level in the solid with respect to the energy levels.

If the electrode is a metal with an atomically flat surface exposed to the electrolyte (Figure 11A), increasing the electrochemical potential leads to the accumulation of electrons in the first atomic layer of the metal and ionic countercharges in the liquid part of the interphase. The study of such a double layer has been a classic subject of electrochemistry, as well as the kinetics of electron transfer between the metal phase and ions in solution.

If the solid phase is a semiconductor or a molecular conductor with a low intrinsic electron concentration (Figure 11B, in which an n-type semiconductor is in contact with an electrolyte), upon increasing the electrochemical potential, the Fermi level in the interfacial layer rises with respect to the conduction band edge. This means that the electron concentration in the interfacial layer increases strongly (Figure 11B, right). It is hence possible to change the electron concentration from almost zero (insulating state) to high values (conducting state) by electrochemical polarization, at least in the interfacial region of the semiconductor.

  

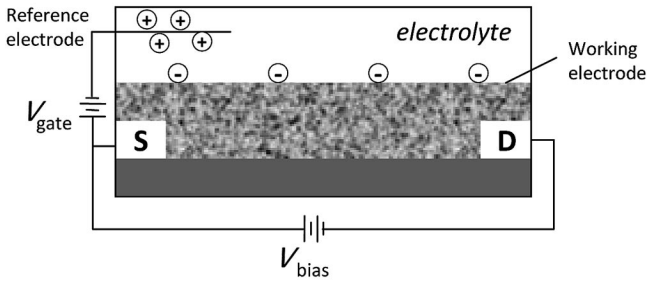


Figure 10. Cell used for electrochemical gating (ECG) of a material. The material of interest is the working electrode. A potentiostat is used to apply a voltage ($V$) between the reference electrode and the working electrode to control the electrochemical potential (Fermi level) of the material. The charge injected into the working electrode is measured in the external circuit. The electronic conductance in the linear regime of the material can be measured independently by applying a small voltage between the source (S) and drain (D) electrodes. Adapted from ref.[147]

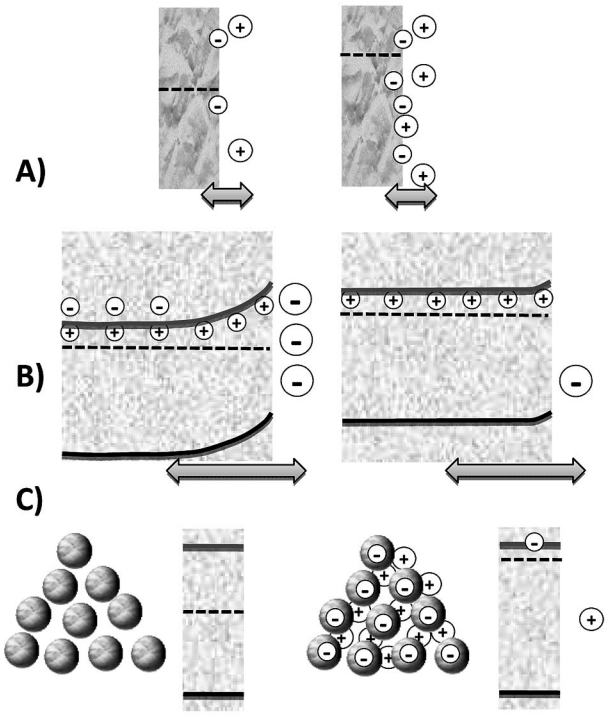


Figure 11. Electrochemical polarization of a solid electronic conductor electrode in a concentrated electrolyte solution. (A) A metal electrode with a flat surface. The arrow indicates the width of the interphase, which is less than 1 nm (concentrated electrolyte solution). (B) Electrochemical polarization of a flat n-type semiconductor electrode. Left: the voltage is chosen such that there is a depletion layer for electrons at the interface. Right: increase in the electrochemical potential leads to a change in the Fermi level with respect to the conduction band edge and an increase in the electron concentration in the interfacial part of the solid. The total width of the interphase (arrow) is typically 100 nm. (C) A semiconductor system with nanometre-size voids in which an electrolyte solution can permeate. Left: system with no excess charge in the solid and liquid phase. Right: increase in the electrochemical potential may lead electrons to occupy the LUMO of the solid phase; the charge is compensated by excess positive ions in the voids. Adapted from ref.[147]

When a nanostructured semiconductor, with pores or voids of nanometre dimensions, is present, the situation is different. Figure 11C, left, shows a situation in which the Fermi level in the solid phase is midway between the HOMO and LUMO orbitals. The solid phase is hence uncharged; this also holds for the electrolyte solution in the voids of the solid that contains as many positive as negative ions. Upon increasing the electrochemical potential, the Fermi level in the solid phase rises with respect to the LUMO. Electrons accumulate in the solid phase and occupy the LUMO energy levels. Alternatively, localized states in the band gap can become occupied. The negative charge in the solid is compensated by an excess of positive ions present in the nanovoids of the system.

In such a nonporous system, the uptake of electrons and hence the capacitance can be huge. Although specific studies are lacking, the nanoarchitecture of the nonporous semiconductor is critical in determining overall behaviour, because the stabilization of the charges within the nanovoids depends on their size and geometry. Charge accumulation within nanocavities would also influence the behaviour of an electrolyte, the diffusion and surface reactivity, i.e. the behaviour as an electrode. There will thus be a true dependence on the nanoarchitecture.

In carbon nanotubes or semiconductor nanowires, electrochemical polarization can also lead to a change in the electron concentration in the tubes or wires,[148] and hence to a significant modification of their properties or those of metal particles supported on them. Due to the presence of anisotropic electron transport in these 1D-type nanostructures, the behaviour of metal particles located on the outer or inner surface would be influenced differently. The electron transport in MWCNTs occurs mainly on the outer shell,[149] but in larger nanotubes a multishell transport may be possible, leading to a quasi-ballistic conducting behaviour, which arises when the electron mean free path is higher than the length of the conductor.[150] It is also well known that there are three main types of carbon nanotubes: armchair, zigzag, chiral. Thus, depending on their type, the transport in nanotubes will also be influenced by the specific structure of the CNT. Therefore, complex phenomena in terms of the influence of the electrochemical polarization on the electrode behaviour may also be expected for carbon nanotubes.

The issue is whether ECG would be a relevant effect during the use of these nanomaterials as electrodes. A nanoelectrode cannot be regarded as an isotropic porous medium, and as a result of the presence of local differences in the potential, electrical shortcuts will be produced, which result in the generation, on a local scale in the presence of an electrolyte, of nano ECG effects. In nanoarchitectured materials, such as in an array of metal oxide nanotubes, it may be expected that these effects play a significant role in determining the overall behaviour. In carbon nanotubes, these effects can also be generated between metal particles located in close proximity, but one sitting on the inner and one on the outer surface of the carbon nanotube. We may thus conclude that ECG effects can be relevant in under-

  

standing the behaviour of nanostructured electrodes, although this can be considered a still largely unexplored field.

There are other aspects, which evidence how the development of nanoarchitectured electrodes opens new issues in the understanding of the physical electrochemistry of these systems. Let us discuss these aspects with reference to DSC devices. As mentioned, these are constituted by colloidal nanocrystals of $TiO_2$, ZnO or $SnO_2$.

Colloidal nanocrystals are usually deposited over a conducting substrate and thermally treated to form a connected array of nanoparticles that can be used as electroactive electrodes. Structures can be more or less ordered, and interparticle connection can also be controlled with molecular ligands, which can be used to promote the self-assembly of special architectures.[151] Alternatively, nanostructured electrodes may be formed from nanofibres or nanowires with columnar, tubular, dendritic or other structures over a substrate. These structures provide longer and uninterrupted paths for electron transport (i.e. reduced intergrain boundaries) with respect to nanoparticle assemblies.[152–155] The presence of an array of vertically aligned nanotubes or nanowires would be useful for a good contact of each of these 1D-type units with the conductive substrate and to reduce the contact between them. Anodic oxidation of a Ti substrate, as shown in Figure 7, is one of the effective synthesis methods to produce ordered arrays of nanotubes. This method has been used in producing transparent $TiO_2$ nanotube arrays for DSCs with high electron lifetimes and excellent pathways for electron percolation.[156]

Additional elements are necessary for the design of efficient DSC devices. An important step of nanostructuring is an additional treatment of colloidal nanoparticles or nanorods for monitoring the electronic properties at the surface. This can be realized, for example, with strategies of conformal coating of sintered nanoparticulate films. Insulating layers (about 2 nm thick) have been deposited over $TiO_2$ nanoparticles in DSCs.[157,158] An alumina coating improves considerably the electron lifetime by an almost complete passivation of surface trap states.[159,160] Absorption of molecules with different dipole moments modifies the energy level of a nanostructured semiconductor immersed in solution.[161] Besides shifting the conduction band of the semiconductor, adsorbed molecules are able to reduce recombination and increase the efficiency of DSCs.[162,163]

Finally, DSC properties can be further improved with surface-attached quantum dots[164] in order to exploit the opportunities arising from discretization of energy levels in quantum dots, which could greatly enhance the photocurrent by multiple exciton generation from a single high-energy photon.[165,166]

The process of electrochemical charging is shown for the DSC in Figure 12. The change in electron density in the $TiO_2$ nanoparticles (by photoinjection from surface-adsorbed dye molecules) is facilitated by positive, but inert, ions at the nanoparticle surface, in order to maintain electrical charge neutrality. Electron density may vary from nearly zero, in the insulator state, to 100 electrons per 10 nm diameter of nanoparticle. In order to generate energy, the electrons should flow through the external circuit and thus avoid the easier path of recombination due to interfacial charge transfer. It follows that an architecture that facilitates a fast vectorial transport of electrons to the conductive substrate, with respect to a random assembly of nanoparticles, could favour the process. This concept is schematically shown in Figure 13.

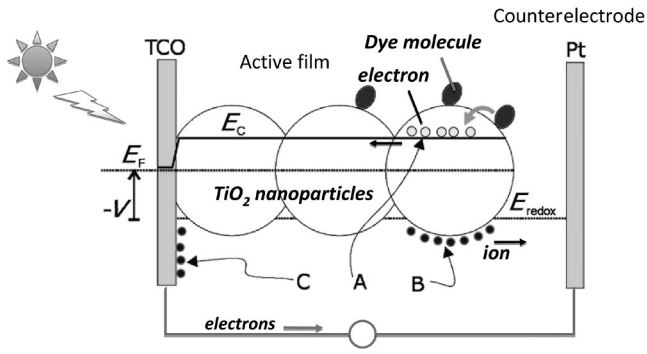


Figure 12. Schematic sketch of a dye-sensitized solar cell, consisting of dye molecules adsorbed on a nanostructured $TiO_2$ (or ZnO, $SnO_2$) film that is deposited over a transparent conducting oxide (TCO). Photoinjection increases the chemical potential (concentration) of electrons in the $TiO_2$ phase (A). The electronic Fermi level, $E_F$, is displaced with respect to the lower edge of the conduction band, $E_c$. The electrode potential, ($V$) is given by the difference between $E_F$ and the redox level $E_{redox}$. The increasing negative charge in the semiconductor nanoparticles is compensated by the positive ionic charge at the surface (B). With the change in $E_F$, the electrostatic potential of the Helmholtz layer also changes, and the semiconductor band bends at the interface between the exposed surface of the transparent conducting oxide substrate and the electrolyte (C). Adapted from ref.[143]

In a thin film of $TiO_2$ nanoparticles, electron transport occurs through trap-limited diffusion, a slow process that allows for back-electron transfer. The concomitant recombination losses limit device efficiencies, especially at longer wavelengths. Electron transport and recombination in $TiO_2$ nanotube arrays limits greatly the recombination of photogenerated charge carriers. The tube geometry allows an active material to be either conformally coated on the walls of the nanotubes or filled into the pores of the semiconductor, which promotes efficient exciton harvesting.

Two approaches are possible for DSCs based on titania nanotube arrays. This field was first explored by Grimes et al.,[63,156,167,168] but attracted great attention from many other groups recently.[169,170] Two types of nanotube arrays, so-called transparent and nontransparent, could be prepared. Nontransparent nanotube arrays are grown on an opaque metallic Ti substrate, while transparent nanotubes are formed by anodizing a Ti film sputtered onto a conductive glass substrate. Opaque nanotubes up to 1 mm in length could be fabricated. However, about 30–40 μm long nanotube arrays are right for optimal light harvest without electron transport losses. The length of transparent nanotubes produced up to now is about 4 μm, but further optimization is possible. Transparent nanotubes lend themselves to front-side illumination, which prevents photonic losses

  

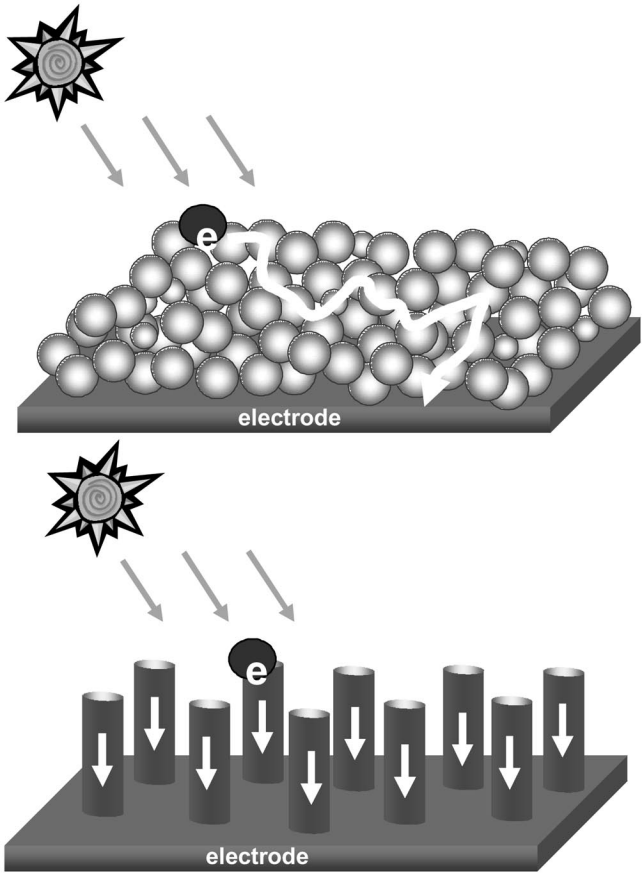


Figure 13. Schematic model of the differences in the electron path between $TiO_2$ thin films composed of nanoparticles and nanostructured in the form of aligned nanorod arrays. Adapted from ref.[24] and ref.[182]

due to absorption by the platinized counterelectrode and the redox electrolyte in DSCs. Backside illumination geometry, where the aforementioned photonic losses occur, is the only mode of illumination possible for nontransparent nanotube arrays. In this mode, part of the light does not arrive at electrode, because it is cut or scattered from the Pt counterelectrodes.

The electron transport times in titania nanotubes are similar to those in nanoparticles, because of the nanocrystalline nature of the tube walls. However, the rate of transport is still much lower than the rate which is possible, for example in carbon nanotubes, for which a ballistic electron transport is even possible, as mentioned before. The incorporation of multiwalled carbon nanotubes (MWCNTs) into a $TiO_2$ active layer contributes to a significant improvement in the energy conversion efficiency of DSCs.[171]

The performance of DSCs using the $TiO_2$–MWCNT composite electrodes is dependent on the MWCNT loading in the electrodes. At optimal conditions, the incorporation of 0.025 wt.-% MWCNTs into the conventional working electrode boosts the efficiency by a factor of up to 1.6. The role of MWCNTs, however, is more complex. In fact, the improvement in energy conversion efficiency is correlated not only with increased photocurrent and electrical double layer capacitance, but also with a decrease in the electrolyte/electrode interfacial resistance and the Warburg impedance. At high MWCNT loading, the conductivity of the electrodes decreases, which may result from the agglomeration of the MWCNTs and the loss of optical transparency.

The other possible approach is to prepare CNT-$TiO_2$ hybrid materials.[172,173] There are many methods to synthesize aligned CNTs.[174,175] A cost-effective method is based on CVD in the presence of volatile Fe complexes, which generate very small iron oxide particles on the substrate on which the carbon nanotubes grow. Figure 14a shows an example of the well-aligned carbon nanotube arrays, which could be synthesized by the CVD method by feeding a $FeCp_2$/toluene mixture. Figure 14b shows that, depending on the duration of the synthesis, different thicknesses of the CNT carpet could be prepared.[176]

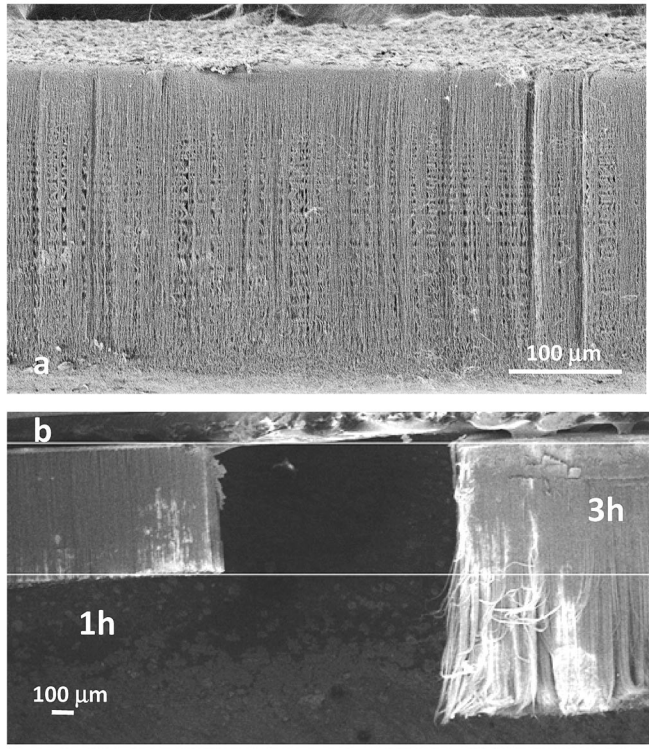


Figure 14. (a) SEM micrographs of the aligned carbon nanotubes synthesized by CVD from a mixture of $FeCp_2$ and toluene at 800 °C. (b) Aligned carbon nanotube carpet with different heights as a function of the duration of synthesis, i.e. 1 and 3 h. The CNT carpet heights were 0.5 and 1 mm, respectively. The growth temperature was kept at 800 °C, and the $FeCp_2$/toluene concentration was 25 g/L. Courtesy of CNRS (LMSPC), Strasbourg (France).

As discussed in Section 2, these CNTs (or carbon nanofibres) could be then loaded or uniformly covered with $TiO_2$ nanoparticles. With respect to the direct use of $TiO_2$ nanotube arrays, the method is more complex, and the density of $TiO_2$ per electrode surface is lower. However, a closer packing could be realized (it is easier to control the aspect ratio, i.e. the ratio between length and diameter, in CNTs), and the electronic conduction is much better. In addition,

  

it is proved that CNTs can change the electronic structure of semiconductors by Fermi equilibrium.[177] It is also demonstrated that chemically modifying n-$TiO_2$ with carbon lowered the band gap of $TiO_2$ to 2.32 eV to make the absorption of visible light possible.[178] Thus, it is possible, in principle, to engineer the band gap of $TiO_2$ by changing the orientation of the graphite sheet, as well as by doping of the carbon nanotubes or nanofibres, which determines the Fermi level of the carbon nanomaterials. However, studies in this direction are still quite limited.

A further possibility is to transform the arrays of aligned CNT or CNF into SiC nanofibres (see Figure 15a) by using a shape-retaining method such as the reaction with SiO vapour.[179] SiC is a semiconductor with a band gap close to that of $TiO_2$, but showing better electronic conductivity properties. This allows to tune the band gap and to realize efficient 1D-nanostructured hybrid materials. It should also be stated that uniform binary and ternary functional inorganic nanotubes are easily fabricated by templating against highly active carbonaceous nanofibres.[180]

A simple methodology of $TiO_2$ deposition on the CNF/CNT arrays is based on a sol–gel/controlled hydrolysis method. The oxide can be deposited both as quantum dots and as a thin film entirely covering the carbon substrate.

Figure 15b shows SEM images evidencing the possibility of depositing uniform and thin entangled $TiO_2$ nanotube films on a macroscopic fibre shape, while Figure 15c schematically shows the mechanism of electron transfer from the $TiO_2$ nanoparticles to the carbon nanotubes.

The size and shape of the $TiO_2$ nanocrystals should influence the mechanism of transfer, although this aspect is usually not considered. If the semiconductor nanocrystallites are wide enough (approximately over 50 nm) so that confinement effects can be neglected, they will have a transport band similar to that for carriers in macroscopic materials. However, the size of $TiO_2$ particles is typically below this range, although full electron confinement is not present. There is thus an intermediate situation between bulk behaviour (electrons injected to the conduction band) and quantum-size effects. The nanomorphology (1D-type, for example) influences the quantum-size effect and thus the electron transfer to a conducting substrate such as a CNT.

If electron confinement could be neglected, the application of a potential will move the electrochemical potential with respect to the value of the electrolyte, and this non-equilibrium situation is the driving force for the flow of electrons. The introduction of discrete states will influence the flow, and thus the nanostructure influences the process. In addition, changes may occur in the local electronic level associated with self-charging of the phase or interaction of the carriers,[181] and also these effects are dependent on the nanostructure. When the DOS (density of states) at the Fermi level is low, the potential has the effect of displacing the Fermi level. In contrast, for metals and highly doped semiconductors, the DOS at the Fermi level is very high. Significant changes in the density of carriers, as an effect of the applied potential, are not possible, because the Fermi level is pinned at a fixed energy.

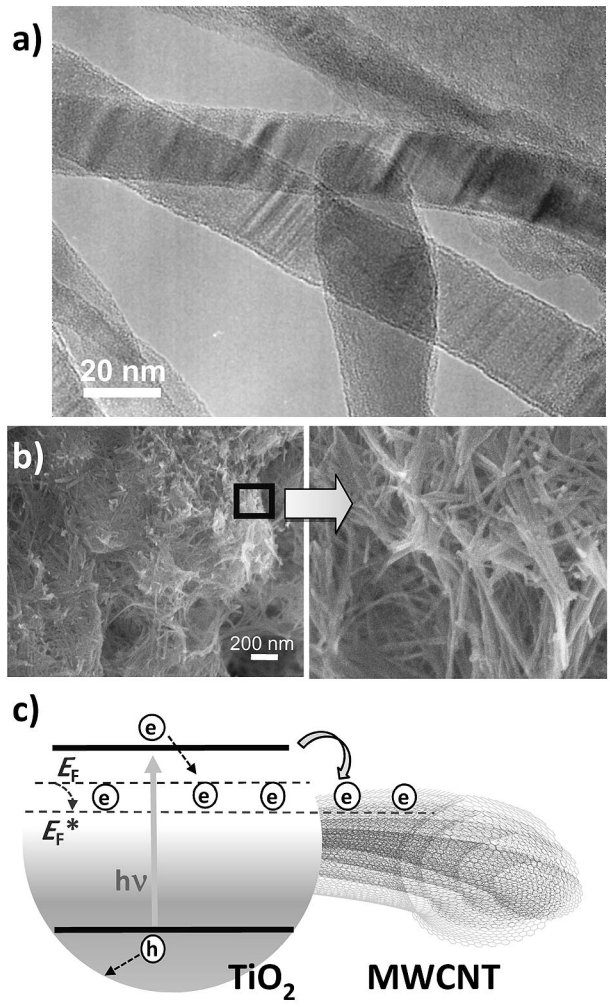


Figure 15. (a) TEM micrograph of the SiC nanofibre formed after a gas–solid reaction between SiO and CNF at 1350 °C. (b) SEM images evidencing the possibility of efficiently depositing uniform and thin entangled $TiO_2$ nanotube films on a macroscopic SiC fibre shape. (c) Schematic model of electron transfer from $TiO_2$ nanoparticles to CNTs. (a) and (b) Courtesy of CNRS (LMSPC), Strasbourg (France). (c) Adapted from ref.[177]

Doping with metal nanoparticles (Au, Ag) is often used in solar cells based on nanostructured semiconductors.[182] Metal particles in contact with a charged semiconductor influence the Fermi levels of the two systems, and the effect is dependent on the size. Au nanoparticles, for example, store electrons in a quantized fashion.[183] When the semiconductor and metal nanoparticles are in contact, the photogenerated electrons are distributed between the two. Since the accumulation of electrons moves the Fermi level of the metal nanoparticle to more negative potentials, the resultant Fermi level of the composite shifts closer to the conduction band of the semiconductor. The apparent Fermi level of the composite system can thus be tuned by controlling the size of the metal nanoparticles. The metal particles thus act both as a sink for electrons to enhance charge separation after photon excitation and as a modifier of the energetics of the system. Consequently, the observed

  

photocurrents at positive bias are significantly higher for the composite films involving Au nanoparticles. Due to the difference in DOS at the Fermi level between a semiconductor and a metal, the application of an electrochemical potential further influences this effect, which is in turn expected to depend on the nanostructure.

The voltage generated by the device is determined by the ability of the different phases to maintain the excess carriers. In solar cells, an electronic connection exists necessarily between the two phases; otherwise, the process of photogeneration would be impossible. Therefore, the kinetics of the reciprocal process (recombination) must be very slow. The nanostructure, as discussed before, plays a critical role in determining the capacity of charge accumulation.

There are thus many aspects related to the nanostructure, whose relevance is amplified when the size of the particles is below about 50 nm and/or when specific nanomorphologies are present. Besides the interfacial processes at the contact of the nanoparticles and the solution, a variety of electronic and ionic processes occur in the material itself.

Some aspects are specifically dependent on the geometry. For example, when an array of semiconductor nanorods is immersed in solution, the outer surface of the rods is depleted of carriers, causing surface band bending in the radial direction, while the central region of the rods is a conducting (quasi-neutral) tubular region connected to the substrate (Figure 16).[143] This structure is ideal for channelling electrons towards the collecting contact, preventing recombination at the surface. The conducting zone in a nanotube is lower (depends on the ratio between wall thickness and depletion layer). The efficiency of electron transport decreases with respect to a nanorod shape. Instead, the conduction mechanism in carbon nanotubes is different, because the CNTs are composed of graphene layers.

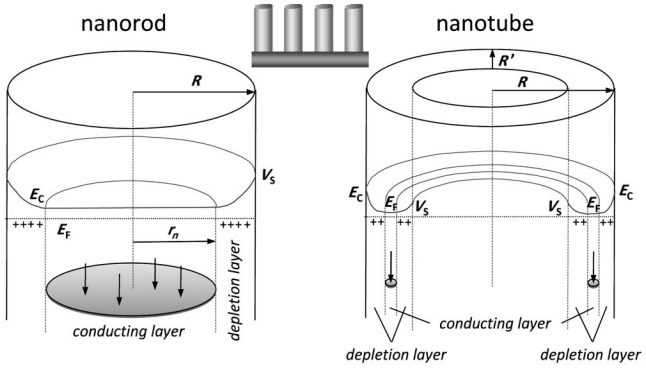


Figure 16. Electrical field and carrier distribution in a semiconductor rod or tube of radius $R$ in contact with electrolyte. $E_c$ is the conduction band energy, $E_F$ is the Fermi level vs. the electric potential at the surface. The surface depletion layer and the central conducting region (radius $r_n$) are indicated. Adapted from ref.[143]

The nanotube geometry is preferable for maximizing the surface area and the amount of dye adsorbed on it, but this contrasts with an efficient electron transport. It is thus preferable (from the electron conduction point of view) to use a hybrid system with a CNT core covered by a titania film or nanoparticles. It should be stated that nanorod-based solar cells, where the 1D nanostructures are based on Cd chalcogenides such as CdSe, CdTe, InP and GaAs, all have excellent properties.[184] Similarly, DSCs based on ZnO nanowire array film also show excellent performance.[185]

Other features also contribute to determine the overall behaviour in relation to the nanostructure. The interfacial charge transfer, which depends on the medium filling the pores, modify the electron lifetimes. However, the transport properties are also affected by an interaction between the electronic carriers in the semiconductor and the surrounding medium. While it has been made possible to control the shift levels by adsorption of molecular species on the surface, the influence of the band gap on the surface states and its relation to electron transport has to be further understood. As a result of the large ratio of surface to volume in nanostructured electrodes, a great amount of surface states are present in the band gap. By decreasing the size and/or changing the nanomorphology, localized states are introduced. This would affect the diffusion of carriers and change the electron transport from a mechanism through extended states (the classical and most widely used mechanism to describe the behaviour also in DSCs),[143] to a transport along discrete energy states and/or localized states (hopping conduction).

The presence of impurities or defects significantly alters the charge transport. The problem is usually treated in terms of slowing down transport through extended states because of trapping/detrapping events,[143] but impurities or defects also introduce localized states and thus also influence the mechanism. In general terms, transport may occur through the bulk of the semiconductor or through the surface, which is inhibited in DSCs by adsorbed molecules. The dyes do not act only as sensitizers of $TiO_2$, but also as efficient quenchers of the surface states. In fact, the dye bonded to the $TiO_2$ surface passivates recombination centres.[186] The suppression of trapping/detrapping events at the surface increases the diffusion coefficient of the electrons through the nanocrystal matrix facilitating electron transport to the back contact.

The size and morphology of nanoparticles influences the presence and localization of impurities and/or defects. An influence, possibly nonlinear, on charge transport is thus expected, but experimental data are limited. In addition, a dispersion of energy levels leads to a scattering of electron waves, which influences the transport. The effect depends on the size and morphology of the nanoparticles. The relationship between the nanostructure of electrodes and charge transport may be thus considered still a largely unexplored area, but which clearly should be at the foundation of a better design of nanostructured electrodes.

Doping of $TiO_2$ with N, C, B or transition metals was widely used to shift the band gap and thus improve titania response to visible light.[187–190] Notwithstanding the intense research and claims of successful visible-light-active photoelectrodes, the improvements are still limited. This is particularly true for demanding reactions such as visible-

  

light water splitting or for the use of these materials as visible-light photoactive anodes. Doping, by introduction of localized trapping levels, completely modifies the electron-transport properties and increases the probability of charge recombination. The gain introduced in terms of a higher number of photons able to photoinduce charge separation is counterbalanced by an increased rate of charge recombination, which reduces the impact of the first effect. Therefore, band gap engineering in semiconductors with an in-depth understanding of the parallel influence on charge transport is requested. The relationship of these aspects with the nanoarchitecture also needs to be understood for progress in this field; results should not only be driven from phenomenological observations.

## 5. Nanostructured Electrocatalysts

In several reviews, the analogy between systems for energy conversion (fuel cell electrodes) and energy storage (supercapacitors, Li-ion batteries) was indicated.[1,2,17,20] There are effective points of contact in their characteristics and design requirements to obtain high-performance electrodes. However, a critical difference is present, which is particularly relevant for the design of the nanostructure of the electrode. In storage devices, a progressive decrease of the capacity is observed, because, for example, $V_2O_5$ reacts with $Li^+$ ions during the discharge process and the opposite process occurs during the charge process [Equation (1)]. In energy conversion devices (fuel cells, for example), an electrocatalytic reaction occurs, i.e. the active element (Pt nanoparticles) is not consumed during the reaction, and a change of the performance during time may occur only due to a (slow) deactivation process.

A PEM fuel cell is composed of an anode, where hydrogen reacts over the active electrocatalyst (Pt nanoparticles supported on carbon) to generate protons and electrons. Protons diffuse through a membrane (such as Nafion) to the cathode, which is electrically connected to the anode through a wire that transports the electrons. At the cathode, oxygen is reduced over the active electrocatalyst (also usually Pt nanoparticles supported on carbon) to form water with the electron and protons coming from the anode.

The kinetics of cathode oxygen reduction on Pt is slow relative to the reaction of hydrogen oxidation at the anode. Therefore, usually it is assumed that the critical issue in PEM cells is to decrease the overpotential of the oxygen reduction reaction (ORR).[13]

Most of the research on PEM electrodes is focused on this problem, which is addressed by using different strategies: (i) increase catalyst activity towards ORR, (ii) increase the utilization of Pt within the electrode through high dispersion of the catalyst and (iii) improve the layer structure of the catalyst, with more limited studies on the role of the nanostructure of Pt particles.[1,5,9,11,13,14,191–199]

Many approaches have been reported for the enhancement of the catalytic activity of Pt towards ORR, as reviewed by Lee et al.[13] In particular, the use of Pt–Me alloys, where Me = Cr, Co, Ni, Fe or other transition metals, has been largely investigated. Ternary alloys were also studied. However, notwithstanding some improvements in the performance, the stability was typically a main issue. More successful is the attempt to improve the utilization of Pt by a proper support engineering.[1,192] For this reason, the research attention has been focused recently on the investigation of the use of advanced nanostructured materials (CNTs, CNFs and others including nanohorns, ordered arrays of CNTs or CNFs, ordered mesoporous carbon).[11,96,193]

We could see that these ORR catalysts are equivalent to those at the anode. Both are based on well-dispersed Pt particles on the same type of nanostructured carbon materials. In commercial cells, the same electrode is often used on both sides. Therefore, although usually the difference between the anode and cathode electrodes is pointed out, we prefer to highlight that the problem of electrode nanoarchitecture is equivalent on the two sides.

$O_2$ reduction to $O^{2-}$ is a four-electron reaction competing with the two-electron reduction leading to $H_2O_2$, which has a negative impact on the lifetime of the cathode and its performance.[200–202] Metalloporphyrins have been often used to promote the four-electron reduction,[201,203] although problems of stability exist. The alternative and preferable approach is to introduce a cocatalyst active for the decomposition of $H_2O_2$ (DHP) to water and oxygen. Zeis et al.[204] have used this approach successfully to develop ORR catalysts based on gold and silver.

For the anode, the issue is how to find a cocatalyst that can introduce a low-temperature water-gas shift (LTWGS) activity, which uses water to oxidize CO to $CO_2$ and produce $H_2$. In fact, even traces of CO severely poison Pt. To improve the CO tolerance of the anode, the presence of a cocatalyst (such as Ru) is necessary, which has the function of promoting CO conversion. In fact, hydrogen is produced by steam reformation of hydrocarbons, and CO is always present in the $H_2$ feed; in actual PEM fuel cells, the concentration of CO must be lower than a few ppm to avoid severe deactivation and drawbacks in performance.

Therefore, a clever approach to electrode design is to consider the anode and cathode not separately, but as two faces of the same problem, which consists of the development of materials with well-dispersed Pt nanoparticles in the presence of a cocatalyst. This function should promote the LTWGS reaction at the anode and the DHP reaction at the cathode. In fact, excellent progress has been made on noble-metal-free electrodes for fuel cells,[205–208] but still high-performance and stable electrodes are based on Pt.

To further strengthen this concept of a unified view of the PEM system, instead of considering the anode and cathode separately, it must be stated that the two electrodes are interconnected and the overpotentials are linked. The strong decrease in the maximum power density when CO is fed (see later) confirms the need of a unitary approach, and it is not appropriate to focus research only on the cathode side.[13,202] We would thus suggest that the electrode design in PEM fuel cells should not be differentiated in terms of

  

anode and cathode, but only in terms of a first level regarding the issue of developing well-dispersed Pt nanoparticles and a second design level related to the efficient introduction of a cocatalytic function.

However, we could also observe that an efficient three-phase boundary should be realized. The electrode design problem is thus not only focused on maximizing the performance of metal nanoparticles by an efficient dispersion, but also on the specific architecture that allows the transport of protons and electrons to or from the metal particles, besides realizing an efficient gas-phase transport of the reactants. The support characteristics (properties and architecture) are important for these aspects. However, it is not always clear that a change in the support properties may influence the electron conductivity of the support or the contact interface ("wettability") with the membrane (Nafion, for example), which, in turn, affects the efficiency of the transport of protons.

Another issue is often not taken into account. If a metal nanoparticle is in poor electronic contact with the carbon substrate, at high current density (when the PEM fuel cell has the maximum power density) charge accumulation occurs on the metal particle. This effect reasonably induces a dynamic particle reconstruction to minimize the surface free energy. Studies on this aspect are limited, but interesting evidence shows the existence of this problem, which is illustrated in the simplified model in Figure 17.

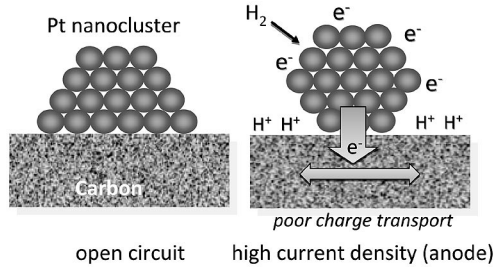


Figure 17. Simplified model to provide evidence for the issue of the reconstruction of Pt nanoparticles in PEM fuel cells during high-current-density operations.

Witkowska et al.[209] investigated by X-ray absorption fine structure (XAFS) analysis an electrode of Pt supported on Vulcan XC-72. XAFS spectroscopy was performed in situ during PEM fuel cell operations. Changes in the near-edge structures reflecting variations in the electronic structure of Pt were observed for different potential values in the activation region. Tada et al.[210] monitored by time-gated rapid XAFS spectroscopy the dynamics of surface changes in Pt nanoparticles during operations in a fuel cell. Kageyama et al.[211] evidenced by in situ XAFS analysis that the local structure around Pt and Ru atoms in the electrocatalysts changes depending on the operation voltage and shows differences in the presence of CO in the fuel gas.

The effect is expected to depend on the size and geometry of the Pt nanoparticles and also on the type of interaction with the carbon support. In addition, in this case, literature data are still preliminary, but they show the importance of this aspect. The scheme reported in Figure 18 summarizes the model derived from combined in situ X-ray absorption near edge structure (XANES) studies and theoretical modelling on the effect of the applied voltage during oxygen adsorption on a Pt/C electrocatalyst. At 0.7 V vs. RHE, O is observed to be adsorbing 1-fold (atop) on Pt, but as the potential is increased, O spills over to an *n*-fold ($n = 2, 3$) configuration. Above 1.0 V, place exchange is observed, and O is observed to go subsurface.[212,213] The electronic effects of H and OH adsorption on Pt/C particles are more extreme on smaller particles than on the larger ones, as evidenced by XANES results. For the larger particles that exhibit a decreased OH adsorption strength, more surface sites are available to perform the oxygen reduction.

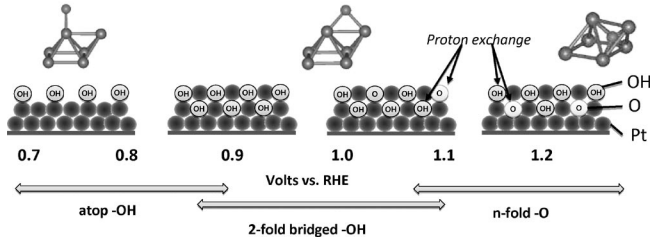


Figure 18. Model of the reconstruction of Pt nanoparticles on carbon by increasing the potential during oxygen reduction in a PEM fuel cell (cathode). Adapted from ref.[212]

Theoretical studies indicate that a reconstruction occurs upon charging the surface. Lozovoi and Alavi[214] investigated the stability of missing-row reconstructions of Pt(110) surfaces with respect to surface charging by using ab initio theory. At small surface charges, the effect of the charge follows the difference of the work functions; i.e., a positive charge favours a surface having a smaller work function and vice versa. Larger charges, either positive or negative, tend to stabilize the reconstructed surface or, more generally, the $1 \times r$ reconstruction with larger $r$. The issue, however, is how to introduce in the calculations the effect of particle size and morphology, as well as the effect of interaction with the substrate.

In nanoparticles, structural and electronic properties strongly depend on size and shape (e.g. quantum size effects; see Figure 19a), and several different types of surface sites are present, which in turn depend on the particle geometry (Figure 19b): steps, kinks, tips, vacancies, etc. When the particle is charged, the surface free energy is influenced, and thus different crystalline planes and/or surface sites are stabilized. The support and its electronic/structural properties influence the size and morphology of the supported particles and its reconstruction. When the full working electrode is considered, a number of further problems arise in modelling, such as the presence of (i) a reactive environment, which might influence the structure, stability and composition of the Pt nanoparticles (or certain functional groups) and (ii) a water layer between the electrode and membrane, which is influenced by the electrical field and affects the adsorption energies stabilizing/destabilizing certain structures.

  

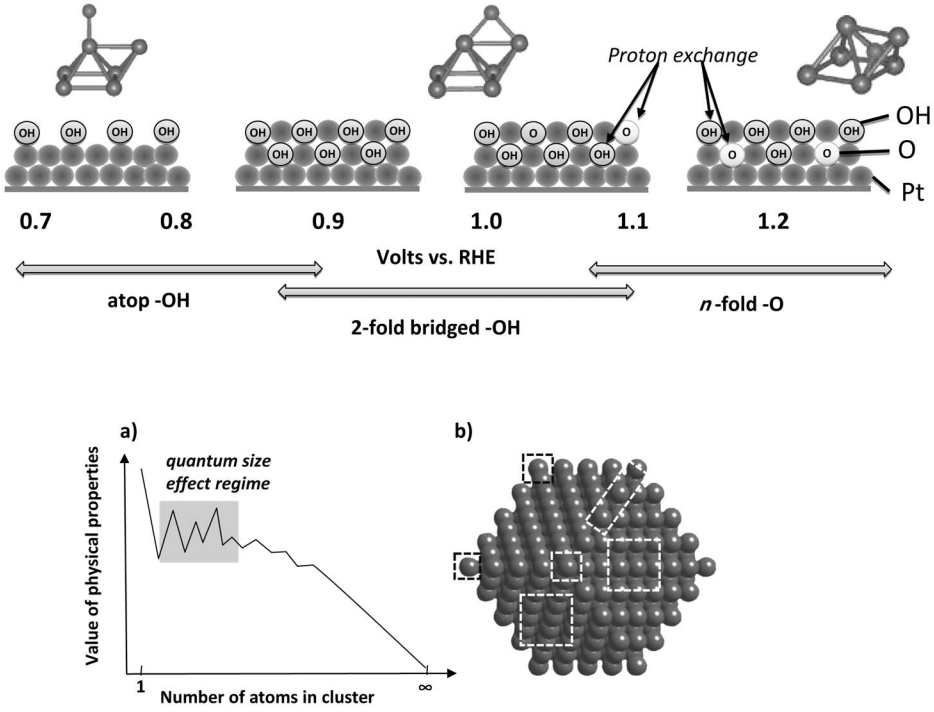


Figure 19. (a) Dependence of the value of physical properties on the number of atoms in clusters; the quantum size effect regime is highlighted. (b) Model of a Pt nanocluster: the different types of surface sites are highlighted.

The adsorption of reactants also induces a reconstruction. The Pt(110) electrode shows a stable $(1 \times 2)$ reconstruction over a wide electrode potential range, and the topmost rows of Pt atoms are expanded into the electrolyte. Additional expansion occurs upon the potential-induced adsorption of hydroxy groups or hydrogen atoms.[215] The presence and stability of the $(1 \times 2)$ reconstruction has an important influence on the surface reactions that can occur in the electrolyte. Recently, these studies have been extended on Pt nanoclusters (37 atoms) supported on carbon.[216] By using density functional theory (DFT) calculations, it was shown that, without hydrogen, the morphology change of a truncated cuboctahedral $Pt_{37}$ is driven by shearing of the (100) to (111) facets to lower the surface energy. With H passivation, the sheared structure automatically reverts to the observed truncated cuboctahedral structure, and the average first-nearest-neighbour Pt–Pt bond length increases by 3. This is due to the preference for H adsorption at bridge sites on (100) facets. However, the preferential sitting of H is influenced by the application of a potential and, in turn, by the reconstruction of Pt nanoparticles.

The interaction with the carbon support would further influence this process. Johnson et al.,[217] showed by DFT calculations that truncated cuboctahedral $Pt_{37}$ clusters supported on graphite evidence the presence of bond-length disorder (in agreement with EXAFS data) arising from anisotropic distortions in the cluster, resulting from interactions of the bottom metal layer in contact with the graphite surface. Figure 20 shows the model of the relaxed structure. Clearly, both the electronic structure of the carbon support and the presence of an applied voltage influence the strength of interface interactions with the clusters and, in turn, its symmetry.

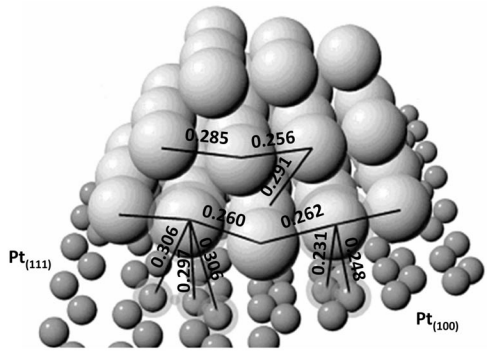


Figure 20. The relaxed structure of a $Pt_{37}$ cluster supported on a graphite surface. Adapted from ref.[217]

The role of the carbon structure in determining the properties of supported noble metal particles is an issue, particularly for the use of novel nanostructured carbons such as CNTs, CNFs, etc. in PEM fuel cells.[1,11,13,192,193,196] CNFs may be grown with different nanostructures (summarized in Figure 21a), depending on the modality of synthesis:[218–221] fishbone, deck of cards and parallel. The fishbone (herringbone; h-CNF) type CNF has graphene layers with an angle of 45° to the growth axis. The deck of cards (platelet; p-CNF) type CNF has graphene layers perpendicular to the growth axis. The parallel (tubular; t-CNF) type CNF has graphene layers parallel to the growth axis with multiwall assembly.

  

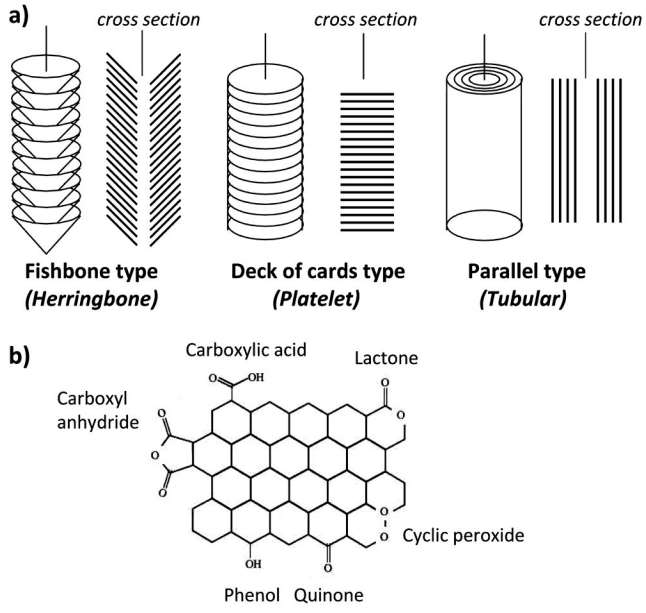


Figure 21. (a) Schematic representation of three types of CNFs. Adapted from refs.[219,220] (b) Types of functional groups produced by the oxidation of carbon.

It was found that noble metals supported on platelet CNFs are more active toward ORR than those supported on fishbone CNFs, both in terms of the onset reduction potential and ORR current peak potentials,[222,223] due to the presence of a higher ratio of edge atoms to basal atoms in platelet CNFs. Tsuji et al.[224] also observed a higher activity of platelet CNF (as support for Pt-Ru nanoparticles) with respect to tubular and herringbone CNF in methanol oxidation.

Depending on the type of CNF and surface nanostructure, different preferential localizations of noble metal particles are present: on the edge of the graphite layers (p-CNF), in the tubes and on the surface (t-CNF), and between the layers and on the edge (h-CNF).[225] The metal nanoparticles show a different activity. The edge atoms of the surface terminating carbon layers are rich in electrons and/or more defective, and they will form different functional groups after the oxidative pretreatment. The latter is made usually prior to the loading of the noble metal. Figure 21b shows the different types of functional groups that can form on the surface of a carbon material. These functional groups will anchor the noble metal particles and thus influence their size (dispersion), stability and reactivity as well.

Masheter et al.[226] have quantitatively determined the amount of quinonyl groups present on the surface with respect to the number of carboxyl groups in "bamboo-like" and "hollow-tube" multiwalled carbon nanotubes (b-MWCNTs and h-MWCNTs, respectively). In the former, the axis of the graphite planes is at an angle to the axis of the nanotubes, and thus the difference between these two types of CNTs is close to the difference between h-CNFs and t-CNFs. In b-MWCNTs, after oxidative pretreatment, the ratio between quinonyl to carboxyl sites is about 6:4, while in h-MWCNT the ratio is 4:6. Also, the total amount of sites is higher in the former.

Therefore, the CNF or CNT nanostructure influences both the dispersion and the reactivity of supported noble metal particles, and their stability as well, because a better interaction with the carbon surface limits Pt mobility and sintering.

However, the nature of the support also influences other properties, which contribute to change the performance of PEM fuel cells. Steigerwall et al.[227] found that Pt-Ru supported on graphitic carbon nanofibres shows better performance as an anode for direct methanol fuel cells than Pt-Ru supported on single-walled nanotubes (SWNTs), multiwalled nanotubes (MWNTs) and herringbone CNFs, and they correlated the behaviour to the electrical conductivity of these four carbon materials. Kim et al.[228] showed that the capacitances of pristine CNFs and surface-modified CNFs could be correlated to the nanostructure. In pristine materials, the edge surfaces of platelet CNFs and herringbone CNFs were more effective in capacitive charging than the basal plane surface of tubular CNFs by a factor of 3–5. Graphitization of p-CNFs changes the edge surface into a dome-like basal plane surface, and the corresponding capacitances decrease. A chemical oxidation, however, recovered a clear edge surface by removal of the curved basal planes. The difference in the contribution of the edge surface and basal-plane surface to the capacitance of CNFs reflects in an anisotropic conduction of graphitic materials.

Another factor that influences behaviour is related to the influence on the proton transport and "wettability" with the proton-transfer membrane (Nafion, for example). As shown in Figure 2, the CNFs or CNTs could be grown over carbon macrofibres (carbon cloth – CC) to realize an efficient nano/micro architecture for PEM electrodes. Li et al.[229] recently proposed the use of carbon nanofibres immobilized on carbon microfibre felts as an efficient system for PEM fuel cell electrodes.

However, there is a problem regarding the contact with Nafion, because a defect-free basal plane has poor contact in comparison with an edge plane. Figure 22 compares the single-cell behaviour of Pt nanoparticles deposited on h-CNTs and p-CNTs grown over CC. The inset of the figure shows a SEM image evidencing the good dispersion of Pt particles with a mean diameter between 2 and 5 nm. There are no remarkable differences in the distribution of Pt particles between h-CNTs and p-CNTs. Single-cell PEM fuel cell tests were performed by using a humidified pure $H_2$ and $O_2$ feed at the anode and the cathode, respectively, with the same commercial E-TEK 20% (wt.-%) Pt catalyst on carbon black/CC at the cathode.[230–232] The tests were run at room temperature (about 20 °C) in order to better observe the problem of contact with Nafion. Figure 22 shows two regions in the polarization curves: region A, where the behaviour is determined mainly by catalysis kinetics and ohmic losses, and region B, where the mass-transfer limitations become dominant. All the other parameters being the same, in this case the behaviour is determined essentially by

  

the limitations in proton mass transport, which are related to the different types of contact between the Nafion membrane and the electrocatalyst. This, in turn, is a function of the "wettability" between the CNFs and the Nafion membrane.

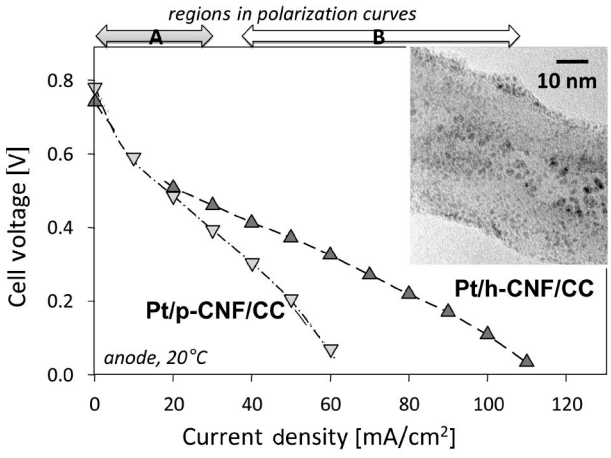


Figure 22. Comparison of the single-cell polarization curves at 20 °C with 20% (wt.-%) Pt supported on h-CNFs and p-CNFs grown over CC. Inset: a SEM image of the Pt/p-CNF/CC sample. For the regions in the polarization curves, see text. As cathode, a commercial E-TEK 20% Pt on Vulcan XC-72/CC was used. Tests were run with with pure $H_2$ and $O_2$ at the anode and cathode, respectively.

The presence of defects on the carbon substrate plays a critical role in all these properties. We can discuss these aspects with a specific example on the comparison of the behaviour of two anode electrodes for a PEM fuel cell based on Pt/MWCNTs, in which in one instance the carbon substrate was subjected to ball-milling prior to the deposition of Pt.[233,234] Ball-milling is a procedure often used to shorten and open multiwalled carbon nanotubes produced by CVD.[235] The process, however, also introduces defects, which may be evidenced by TEM images.[234] During ball-milling, the frequent collisions and the high velocity of the steel balls cause strong impacts on the nanotubes. If the collision energy is high enough, the cylindrical structure of the CNTs is cracked at the impact sites, and the graphene layer breaks down. Therefore, short nanotubes with open ends can be formed. Milled nanotubes are prone to break at the sites of structural defects, such as bends, thus causing the majority of milled CNTs to be straight. In addition, if the intensity of collisions is not high enough to cause nanotube cleavage, they will produce more defects on the tube walls.

Defects in CNTs are usually introduced by an oxidation pretreatment with nitric acid, $H_2O_2$ or other reactants. The treatment is necessary to obtain a good dispersion of the metal particles. These methods, in fact, create different surface functional groups (lactone, pyran, carboxyl, anhydride, quinone, phenol, furan) (see Figure 21b), although several of these groups have a low thermal stability. The type of pretreatment influences the dispersion and electrocatalytic activity,[236] but often results are only phenomenological. In addition, other types of defects not associated to oxidation treatments could be present in CNTs, such as vacancies, vacancy-related defects or nonhexagonal carbon rings.[237] These topological defects may occur in the as-grown nanotubes, or they can be generated by several methods like chemical treatment, mechanical or irradiation treatment. The ball-milling may thus be considered as a method to create mechanically induced topological defects in CNTs, which are able to anchor efficiently Pt nanoparticles. We call the nondefective and defective samples hereafter Pt/*nd*-CNT and Pt/*d*-CNT, respectively.

The presence of defects improves the dispersion of Pt particles. The average size of Pt particles in Pt/*d*-CNTs is 1.4 nm, while the particle size in Pt/*nd*-CNTs shows a bimodal distribution, centred at 1 nm and 4.5 nm. The average size of Pt particles in Pt/*nd*-CNTs is 3.0 nm. For reference, the mean size of Pt particles in Pt/Vulcan XC-72 electrocatalysts was found to be about 3.6 nm.[238] Therefore, in both Pt/*d*-CNTs and Pt/*nd*-CNTs, small Pt nanoparticles (<2 nm), with size below the usual observed in Pt/carbon black materials are the dominant species. However, a uniform distribution is observed in the Pt/*d*-CNT sample. The distribution of Pt particles allows estimating the geometrical surface area (GSA) of Pt particles on the basis of the assumption of a round-shaped geometry. The results are summarized in Table 1, using both the mean diameters of the particles and the size distribution. For Pt/*d*-CNTs the difference is minimal, but in Pt/*nd*-CNTs, where a broader and bimodal particle size distribution is present, the difference is relevant. The GSA is usually estimated only on the basis of the mean diameter of the Pt particles.

Table 1. Electrochemical active surface area (EAS) determined by cyclic voltammetry experiments, geometrical surface area (GSA), estimated on the basis of the mean diameter of Pt particles or the size distribution determined by TEM measurements, and the mean value of the ratio of the EDX peak intensities of F and Pt in the SEM images of the Pt/CNT/CC/Nafion composite. Adapted from ref.[234]

| Sample | EAS [$m^2$/g] | GSA [$m^2$/g][a] | GSA [$m^2$/g][b] | F/Pt[c] | $R$ [V/mA][d] |
|---|---|---|---|---|---|
| Pt/*d*-CNT | 163.3 | 200.3 | 207.6 | 1.3 | $3.329 \times 10^{-3}$ |
| Pt/*nd*-CNT | 114.3 | 93.5 | 151.8 | 0.8 | $4.490 \times 10^{-3}$ |

[a] Based on mean diameter. [b] Based on size distribution. [c] Average value of about 20 measurements (different spot zones) of the local ratio between the intensities of the EDX peaks of F (related to Nafion) and Pt in the SEM measurements of the membrane electrode assembly (MEA). [d] Ohmic resistance in the Tafel plot.

The geometrical surface area determined from the particle size is an indication of the total available surface area, which depends on the dispersion of Pt on the support. However, it does not provide an estimation of the electrochemical active surface area. In fact, part of the Pt particles may be inactive, because of poor contact with the carbon conductive substrate or because part of the surface area is not accessible to the gas reactants. The estimation of the

  

electrochemical active surface area (EAS) can be made by cyclic voltammetry (CV) experiments in acid solution to calculate the amount of charge transfer during the electroadsorption and -desorption of $H_2$ on Pt sites.[239] The values should be corrected for the contribution of double-layer charge and eventually of the support.

The values of the EAS estimated in this way are also reported in Table 1. It may be noted that the EAS is about 20–25% lower than the GSA, a result which is consistent with literature observations. Cai et al.,[238] for example, found that the percentage of Pt utilization, i.e. the ratio between EAS and GAS (indicated by them as chemical surface area – CSA), is about 80%. Considering that it is reasonable to assume a contact angle of about 130–150° (with respect to 180° for an ideal round-shaped Pt particle without interaction with a flat carbon surface), from simple geometrical considerations, it is possible to estimate that at least 20% of the ideal geometrical surface of Pt nanoparticles is not accessible to hydrogen adsorption. The data on EAS thus indicate that nearly all the Pt nanoparticles are accessible to hydrogen adsorption and electrochemical reaction. On the basis of EAS determination, the activity of Pt/*d*-CNTs should be about 30% higher than that of Pt/*nd*-CNTs.

CV data[234] provide further indications on the difference between the two samples. Maruyama and Abe,[240] who studied the behaviour of glassy carbon (GC) electrodes by cyclic voltammetry, where the surface was electrochemically oxidized to generate hydrophilic groups, showed that surface functional groups, such as quinone-like groups, contribute to determining the shape of CV curves in acid medium. When the degree of surface oxidation increased, the current in both anodic and cathodic scans increased, and a broad peak centred at around 0.35 V (with respect to SCE) both in the anodic and cathodic sides of the CV graph were observed. These peaks were caused by the redox reaction of quinone-like functional groups on the GC surface [Equation (4)].

$$C{=}O + 2H^+ + 2e^- \leftrightharpoons C(OH)_2 \quad (4)$$

The CV curve of Pt/*d*-CNTs shows clearly this contribution, which is instead minimal in Pt/*nd*-CNTs, confirming that ball-milling induces the formation of a large number of surface defects on CNTs.

The presence of defects, however, does not influence only the size and dispersion of Pt particles. An important aspect regards the efficiency of the three-phase boundary and particularly the efficiency of the transport of protons generated during $H_2$ oxidation (see also Figure 17). The contact between the Pt/CNTs and the Nafion membrane is not easy to estimate, but in SEM images of the assembled electrode (MEA – membrane electrode assembly) it is possible to measure the ratio between EDX intensities of Pt and F (Nafion is a sulfonated, tetrafluoroethylene-based fluoropolymer copolymer). By averaging the measure over several local spots, it is possible to have an indication of the effectiveness of the contact. The results in Table 1 show that this ratio is about 40% higher in Pt/*d*-CNTs with respect to Pt/*nd*-CNTs. This is due to the presence of a higher number of defects, and associated functional groups in the former allow a better contact with the Nafion.

Another important aspect to consider is the electron transfer resistance of the CNT substrate, which influences the charging effect of the Pt nanoparticles during high-current-density operations (see Figure 17). Also in this case, direct measurements are not easy, but an estimation is possible by analyzing the polarization curves in single-cell experiments in terms of the modified Tafel equation.[241] [Equation (5)].

$$E = E^\circ - b\log i - iR \quad (5)$$

$E$ is the cell potential, $i$ the current density, $b$ the so-called Tafel slope and $R$ is predominantly the ohmic resistance in the electrode and electrolyte responsible for the linear variation of potential vs. current density plot. $E^\circ$ is related to the exchange current density, $i^\circ$, as shown in Equation (6).

$$E^\circ = E_r + b\cdot\log i^\circ \quad (6)$$

$E_r$ is the reversible potential for the anode reaction.

The kinetic parameters in Equation (5) could be estimated from the experimental data by a nonlinear least-squares regression analysis. The resulting values show that $E^\circ$ is similar for the two Pt/CNT samples, indicating that the exchange current ($i^\circ$), which is related to the reaction kinetics, is nearly the same. The value of $R$ (Table 1) is about 25% higher for the Pt/*nd*-CNTs with respect to Pt/*d*-CNTs. $R$ is related to the ohmic resistance and depends on many parameters. However, all conditions of preparation are the same, apart from the nature of the CNTs. The differences observed for the single-cell performances are reproducible when the samples are prepared again, and thus the difference in the $R$ value is related to the different electronic conduction of the CNTs.

Therefore, the nature of CNTs and the presence of defects influence many aspects, not only the dispersion of Pt and the related electrochemically active surface. There is an influence on the (i) efficiency of the contact with Nafion and thus on the proton transfer and effectiveness of the three-phase boundary, as commented above, (ii) resistance to electron transfer, as indicated by the different value of the $R$ parameter in Table 1, and (iii) specific characteristics of the Pt particles. The latter differ not only in terms of dispersion, but also in terms of the interaction between the carbon substrate and the metal particles, which in turn influences the specific characteristics and reactivities of the supported Pt particles. In fact, the maximum power density determined in single-cell experiments with pure $H_2$ and $O_2$ feeds at the anode and cathode shows a value about 65% higher for Pt/*d*-CNTs with respect to that for Pt/*nd*-CNTs. The increase in the maximum power density is significantly larger than that expected from the differences in the electrochemical surface area (Table 1), confirming that additional effects are present.

  

When CO is present together with $H_2$ in the anode feed, a lowering of the performance of PEM fuel cells is shown due to the strong chemisorption of CO on the Pt sites, which inhibits the electrochemical activity in $H_2$ oxidation to protons and electrons. It is thus interesting to analyze whether the presence of defects in CNTs influences differently the behaviour of the two samples with respect to that of the experiments with pure $H_2$ flow at the anode.

The maximum value of the power density (MPD) of Pt/*d*-CNTs decreases from about 28 to 24 mW/cm$^2$ upon addition of 50 ppm CO to the $H_2$ feed, i.e. a decrease of less than 15%. On the contrary, the MPD of Pt/*nd*-CNTs decreases more than 50% in the presence of CO. These experiments were carried out at low temperature (20 °C), in order to avoid limitations at the cathode. Therefore, the maximum value of the power density is limited, but in line with that observed for commercial Pt/carbon black samples.[244]

It is necessary to analyze whether the maximum power density (MPD) correlates only with the presence of small Pt nanoparticles in Pt/CNT samples. By using the experimental distribution of Pt particles, the fraction of the total surface area that can be attributed to particles below a critical size (1.5 nm in diameter, for example) can be calculated. From this value, the electrochemical active surface area (EAS) of these particles is estimated by multiplying this fraction by the total measured EAS. This EAS for particles below 1.5 nm may then be put in relation with the MPD value for single-cell tests with or without the presence of CO in the $H_2$ flow. The results are summarized in Figure 23.

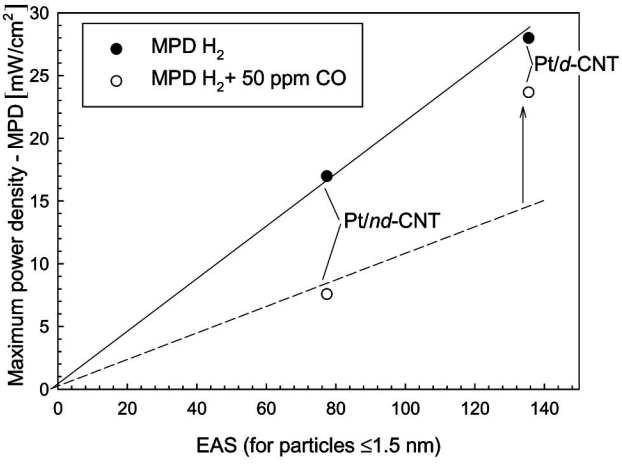


Figure 23. Relation between electrochemical active surface area (EAS) for particles of diameter less than or equal to 1.5 nm (see text) and maximum power density (MPD) for single-cell experiments with pure $H_2$ or $H_2$ and CO (50 ppm) feeds at the anode. Single-element PEM fuel cell: E-TEK Pt/Vulcan XC-72 on CC was used as the cathode to which oxygen saturated with $H_2O$ at room temp. was fed. Nafion® 115 was used as the membrane. Room temperature (20 °C), 1 atm, feed of pure $H_2$ (saturated at room temp. with $H_2O$) at the anode.

Assuming as active only the particles of diameter less than or equal to 1.5 nm, a linear relationship is observed for the $H_2$ case, but not when CO is present in the feed. This evidences not only the role of CNTs in determining the dispersion of supported Pt particles, but also the presence of additional effects in the experiments with CO.

It is known that the CO tolerance of Pt-Ru electrocatalysts is related to the formation of Brønsted acid sites (due to water activation) that catalyze the oxidation of CO.[242,243] CV tests have evidenced the higher abundance of surface functional oxygen-containing groups on *d*-CNTs, which reasonably act also as anchoring sites for the Pt nanoparticles. These sites could assist in CO oxidation and thus improve the CO tolerance of the electrocatalysts, particularly when very small Pt nanoparticles (<2 nm) are present, as in the discussed Pt/CNT samples.

Many factors contribute to the single-cell behaviour. It is thus necessary to consider the complexity of these phenomena in analyzing the use of carbon nanotubes in advanced electrodes. The results also evidence that specific attention should be paid to the role of defects, taking into account that they influence several aspects of the physical electrochemistry of the materials and not only the dispersion of Pt particles, as often assumed.

A final important consideration regards the influence of defects on the durability of electrocatalysts supported on CNFs or CNTs, a relevant issue for practical applications.[244,245] The corrosion of carbon materials usually initiates at defect sites.[246,247] Therefore, the presence of defects is beneficial on one side, but could be negative on the other side. However, data on the role of defects in CNT/CNF and electrode stability are quite limited. Shao et al.,[245] analyzing the effect of the use of CNTs, concluded that they improve the durability of catalysts for PEM fuel cells with respect to Vulcan XC-72 carbon black. This was related only to the higher resistance of CNTs towards surface oxidation with respect to carbon black.[248] This property depends clearly on the specific CNT characteristics and the number of defects as well.

On the other hand, the number and type of defects also influence the rate of Pt ripening and anchorage to the support. In fact, there are two mechanisms of sintering of Pt particles, particularly under application of a potential: (a) Ostwald ripening on carbon at the nanometre scale and (b) migration of soluble Pt species in the ionomer phase at the micrometre scale, chemical reduction of these species and crossover over the membrane, and finally, precipitation of Pt particles in the cathode ionomer phase, which reduces the amount of Pt on C.[249] Moreover, a stronger interaction of Pt with the CNF surface with respect to that of carbon black was reported,[247,250] although not related to the specific nature of surface functional groups.

Grolleau et al.[251] recently reported the behaviour of Pt particles dispersed on two different Vulcan XC72 carbon supports. One was used after thermal treatment at 400 °C under a nitrogen atmosphere, the other after oxidation of its surface by $HNO_3$. TEM results indicated that the mean particle size was a little higher on the non-oxidized support (Pt/XC72) than that on the functionalized one (Pt/XC72 $HNO_3$), 2.5 and 2.0 nm, respectively. However, potential cycles from 0.05 to 1.25 V vs. RHE led to a higher increase

  

in the particle size when the catalyst was dispersed on the functionalized support, reaching after 400 potential cycles 5.5 nm versus 4.0 nm with the nonfunctionalized one. These results indicate a negative role of the oxidized functional groups on the Pt sintering upon potential cycling. On the other hand, the results cannot be extrapolated to CNTs or CNFs, because of the different nanostructure of carbon black and the presence of sulfur, as well. Therefore, the question of whether the carbon nanostructure influences positively or negatively the stability of PEM electrodes is still open.

It must be finally cited that a new interesting area of development is the direct nanostructuration of noble metals. Chien and Jeng[14] proposed a 3D nanonetwork of Pt and Pt-Ru catalysts for cathode use in direct methanol fuel cells (DMFC). The catalysts are prepared in the void spaces of a self-assembled, layered template of polystyrene (PS) nanospheres by chemical reduction deposition. Removal of the template by thermal decomposition resulted in the formation of a nanonetwork catalyst with sizes of network frames and hollow holes of around 10–200 nm. Physical and electrochemical characterizations demonstrated that such nanostructured catalysts have distinctive characteristics including robust structures, spacious hollows, connected flow channels, large surface areas and high electrocatalytic activities. The prepared Pt and Pt-Ru nanonetwork catalysts were applied to a single-cell DMFC as cathode and anode catalysts, respectively, with a low catalyst loading of 0.2 mg/cm$^2$ for each. Results indicated that a good cell performance is obtained with high normalized power densities. The maximal normalized power density at 60 °C was about 3–4 times that of a DMFC used for comparison that had conventional catalysts with a high catalyst loading of 4.0 mg/cm$^2$. However, substantial improvements are still required, in both catalyst loading and electrode size, for more practical applications.

Sun et al.[199] instead investigated the use of Pt nanowires on carbon black for the oxygen reduction reaction (ORR) in PEM fuel cells. The addition of carbon black to an aqueous solution of $H_2PtCl_6$ and HCOOH resulted in the direct growth of Pt nanowires on the nanospheres of the carbon support. In these nanostructures, the high-surface-area carbon black (Vulcan XC72) serves as the core, and the electrocatalytically active Pt nanowires are grown radially from the surface of the carbon particles. These Pt nanowire/C nanocomposites show enhanced catalytic activity for the ORR relative to a state-of-the-art Pt/C catalyst made of Pt nanoparticles. The surface of carbon spheres is densely covered by packed arrays of Pt nanowires. Most of the nanowires are 10–30 nm in length, but some of them can reach up to a hundred nanometres. Some nanowires assemble into flower-like 3D superstructures on carbon spheres. No data have been reported on stability, which could be a problem for this type of electrocatalysts.

Other authors investigated the use of electrodes based on Pt nanowires,[252–256] observing in general interesting properties related to the unique physicochemical and electronic properties arising from the inherent anisotropic 1D nanostructure, such as charge-transfer facilitation, more efficient use of Pt and a better interface.

Metallic nanowires could be produced also by using mesoporous materials as template. Choi and Woo[257] reported the synthesis of Pt-Ru nanowires with SBA-15 as template and compared them with the behaviour of commercial Pt-Ru black. TEM and XRD data of the synthesized material show that in this network structure the Pt-Ru nanowires are interconnected through smaller ones. The catalytic activity, measured by cyclic voltammetry (CV) for MeOH electrooxidation on this material, is lower than that of commercial Pt-Ru black at potentials below 550 mV vs. RHE. In contrast, a direct-MeOH fuel cell with the nanostructured product as anode material shows a higher performance than that of a cell with Pt-Ru black, because the network structure leads to effective mass transfer in the membrane electrode assembly.

Zhao et al.[258] instead synthesized a Pt nanowire array electrode by electrodeposition of Pt into the pores of an anodic Al oxide (AAO) template. TEM analysis showed that the nanowires have a uniform diameter of about 30 nm. The brush-shaped Pt nanowire array electrode can be seen by field emission SEM. The Pt nanowire array electrode showed good performance in the electrooxidation of MeOH. Chen et al.[259] proposed a new class of cathode catalysts based on supportless Pt and Pt-Pd nanotubes. These materials have good durability and high catalytic activity. These catalysts may overcome the degradation that affects current Pt/C and Pt-black catalysts.

The nanostructuration of Pt, in the form of nanowires or 3D nanonetworks is thus a novel, interesting area in the field of PEM fuel cells, particularly for direct alcohol applications. A better understanding of the role of nanoarchitecture, however, is necessary.

## 6. Conclusions and Perspectives

The field of nanostructured electrodes for applications ranging from energy storage (Li-ion batteries, supercapacitors) to energy conversion (fuel cells, solar devices) is an area of growing interest from both the fundamental and the application points of view. This microreview examines a series of selected aspects related to the role of nanostructure and nanoarchitecture in novel Li-ion batteries, solar devices and fuel cells based on metal oxides ($TiO_2$, $V_2O_5$), carbon nanotubes and nanofibres and their hybrid materials, as well as their use to support noble metal particles.

Notwithstanding the great progress made in these fields in the recent years, it is notable that the decrease in the size to nanodimensions opens new problems in understanding. The developments have been in large partly driven by phenomenological investigations and were material-oriented. The next necessary step is a more in-depth understanding of the complex phenomena at the foundation of the physical electrochemistry and reaction/transport kinetics during the operation of the systems. Some of the areas in which a better understanding is necessary have been highlighted.

  

It was also evidenced that many simultaneous effects contribute to determining the overall behaviour and thus the optimization of the performance and nanoarchitecture of the materials requires understanding this complexity.

In conclusion, this is an exciting area of inorganic chemistry with relevant implications to implement sustainable energy. Together with catalysis, with which it shares many aspects, it is one of the fields of nanomaterials, which can better demonstrate the direct link between progress in nanodesign and benefits in terms of large-scale applications. However, further progress in the area can be achieved only with a better understanding of the relationship between hierarchical organization and nanosize-dependent effects and performance.

This would require the integrated use of several advanced physicochemical characterization methods, but the key development is to emphasize the use of in situ methodologies to characterize the nanomaterials in the presence of an applied voltage and a reactive environment. Significant progresses has been made recently in the field of heterogeneous catalysis, and these results should be used to characterize the behaviour of electrodes. In addition, many of the processes are time-dependent, and thus time-resolved characterization techniques have to be used. Initial interesting attempts in this direction show the need to progress in this area.

It is also necessary to progress in the real understanding of the role of nanoarchitecture on the reactivity and performance of these electrodes by the development of more focused methodologies. The need for a better understanding of charge transport in relation to nanostructure has to be pointed out, in particular.

## Acknowledgments

This work has been realized in the frame of ELCASS (European Laboratory for Catalysis and Surface Science) in which the Centre National de la Recherche Scientifique (CNRS)/Universitè Louis Pasteur (ULP) of Strasbourg, France, the Fritz Haber Institute of the Max Planck Society (FHI-MPG) of Berlin, Germany and the University of Messina, Italy participate. The collaboration of Dr. D. S. Su and Prof. R. Schlögl (Berlin), and Dr. C. Pham-Huu (Strasbourg) in particular, is gratefully acknowledged.

[1] J. Liu, G. Cao, Z. Yang, D. Wang, D. Dubois, X. Zhou, G. L. Graff, L. R. Pederson, J.-G. Zhang, *ChemSusChem* **2008**, *1*, 676–697.
[2] Y.-G. Guo, J.-S. Hu, L.-J. Wan, *Adv. Mater.* **2008**, *20*, 2878–2887.
[3] Y. Xie, C. Wu, *Dalton Trans.* **2007**, 5235–5240.
[4] A. Gotcher, *Adv. Mater. Processes* **2005**, *163*, 32–33.
[5] J. J. Gooding, *Electrochim. Acta* **2005**, *50*, 3049–3060.
[6] Y.-G. Guo, Y.-S. Hu, W. Sigle, J. Maier, *Adv. Mater.* **2007**, *19*, 2087–2091.
[7] A. Singhal, G. Skandan, G. Amatucci, F. Badway, N. Ye, A. Manthiram, H. Ye, J. J. Xu, *J. Power Sources* **2004**, *129*, 38–44.
[8] P. Simon, Y. Gogotsi, *Nat. Mater.* **2008**, *7*, 845–854.
[9] A. Eftekhari (Ed.), *Nanostructured Materials in Electrochemistry*, Wiley-VCH, Weinheim, **2008**.
[10] R. L. McCreery, *Chem. Rev.* **2008**, *108*, 2646–2687.
[11] C. Liu, H.-H. Cheng, *J. Phys. D: Appl. Phys.* **2005**, *38*, R231–R252.
[12] D. S. Mainardi, N. P. Mahalik, "Nanotechnology for Fuel Cell Applications" in *Micromanufacturing and Nanotechnology* (Ed.: N. P. Mahalik), **2006**, Springer, Berlin, pp. 425–440.
[13] K. Lee, J. Zhang, H. Wang, D. P. Wilkinson, *J. Appl. Electrochem.* **2006**, *36*, 507–522.
[14] C.-C. Chien, K.-T. Jeng, *Mater. Chem. Phys.* **2007**, *103*, 400–406.
[15] P. G. Bruce, B. Scrosati, J.-M. Tarascon, *Angew. Chem. Int. Ed.* **2008**, *47*, 2930–2946.
[16] K.-W. Park, Y.-E. Sung, *J. Ind. Eng. Chem.* **2006**, *12*, 165–174.
[17] D. R. Rolison, J. W. Long, J. C. Lytle, A. E. Fischer, C. P. Rhodes, T. M. McEvoy, M. E. Bourg, A. M. Lubers, *Chem. Soc. Rev.* **2009**, *38*, 226–252.
[18] H. Zhang, J.-J. Xu, H.-Y. Chen, *J. Phys. Chem. C* **2008**, *112*, 13886–13892.
[19] Y.-G. Guo, H.-M. Zhang, J.-S. Hu, L.-J. Wan, C.-L. Bai, *Thin Solid Films* **2005**, *484*, 341–345.
[20] A. S. Aricò, P. Bruce, B. Scrosati, J.-M. Tarascon, W. van Schalkwijk, *Nat. Mater.* **2005**, *4*, 366–377.
[21] J. Majer, *Nat. Mater.* **2005**, *4*, 805–815.
[22] L. F. Nazar, G. Goward, F. Leroux, M. Duncan, H. Huang, T. Kerr, J. Gaubicher, *Int. J. Inorg. Mater.* **2001**, *3*, 191–200.
[23] G. Centi, S. Perathoner, *Catalysis* **2007**, *20*, 367–394; J. J. Spivey (Ed.), *Nano-archictecture and reactivity of titania catalytic materials – Quasi-1D nanostructures*, Royal Society of Chemistry Pub., Cambridge, **2007**.
[24] G. Centi, S. Perathoner, *Catalysis* **2008**, *21*, 1–39; J. J. Spivey (Ed.), *Nano-architecture and reactivity of titania catalytic materials – Part 2* ("Bidimensional nanostructured films"), Royal Society of Chemistry Pub., Cambridge, **2009**, vol. 21, p. 82–130.
[25] X. Zhang, J. Sun, J. Shen, *Multilayer Thin Films* (Eds.: G. Decher, J. B. Schlenoff), **2003**, Wiley-VCH, Weinheim, Germany, pp. 301–330.
[26] D. R. Rolison, J. W. Long, J. C. Lytle, A. E. Fischer, C. N. Chervin, K. A. Pettigrew, M. J. Geselbracht, M. P. Saunders, "Architectural Design, Interior Decoration, and 3-D Plumbing En Route to Multifunctional Nanoarchitectures – Especially for Energy Storage and Conversion", presented at the 235th ACS National Meeting, New Orleans, LA, United States, April 6–10, **2008**, IEC-027.
[27] J. W. Long, A. E. Fischer, J. C. Lytle, K. A. Pettigrew, D. R. Rolison, "Multifunctional Carbon Nanoarchitectures As Designer Platforms for Electrochemical Power Sources", presented at the 235th ACS National Meeting, New Orleans, LA, United States, April 6–10, **2008**, COLL-486.
[28] J. W. Long, D. R. Rolison, *Acc. Chem. Res.* **2007**, *40*, 854–862.
[29] A. M. Cao, J. S. Hu, H. P. Liang, L. J. Wan, *Angew. Chem. Int. Ed.* **2005**, *44*, 4391.
[30] C. R. Sides, C. R. Martin, *Adv. Mater.* **2005**, *17*, 125–128.
[31] D. Sun, C. W. Kwon, G. Baure, E. Richman, J. MacLean, B. Dunn, S. H. Tolbert, *Adv. Funct. Mater.* **2004**, *14*, 1197–1204.
[32] J. Schoonman, NATO Science Series, II: Mathematics, Physics and Chemistry, **2005**, Vol. 204 (Nanostructured and Advanced Materials for Applications in Sensor, Optoelectronic and Photovoltaic Technology), pp. 259–270.
[33] L. Schmidt-Mende, J. L. MacManus-Driscoll, *Materials Today* (Oxford, UK), **2007**, *10(5)*, 40–48.
[34] J. W. Fergus, *J. Mater. Sci.* **2003**, *38*, 4259–4270.
[35] Q. Zhang, S.-J. Liu, S.-H. Yu, *J. Mater. Chem.* **2009**, *19*, 191–207.
[36] B. C. Satishkumar, A. Govindaraj, *J. Mater. Chem.* **2000**, *10*, 2115–2119.
[37] I.-H. Kim, J.-H. Kim, B.-W. Cho, Y.-H. Lee, K.-B. Kim, *J. Electrochem. Soc.* **2006**, *153*, A989–A996.
[38] W.-C. Fang, W.-L. Fang, *Chem. Commun.* **2008**, *41*, 5236–5238.
[39] W.-C. Fang, *J. Phys. Chem. C* **2008**, *112*, 11552–11555.

  

[40] X.-W. Chen, Z. Zhu, M. Haevecker, D. S. Su, R. Schlögl, *Mater. Res. Bull.* **2007**, *42*, 354–361.

[41] M. Gangeri, G. Centi, A. La Malfa, S. Perathoner, R. Vieira, C. Pham-Huu, M. J. Ledoux, *Catal. Today* **2005**, *102–103*, 50–57.

[42] B. Louis, G. Gulino, R. Vieira, J. Amadou, T. Dintzer, S. Galvagno, G. Centi, M. J. Ledoux, C. Pham-Huu, *Catal. Today* **2005**, *102–103*, 23–28.

[43] Z. Zhu, D. S. Su, G. Weinberg, R. E. Jentoft, R. Schlögl, *Small* **2005**, *1*, 107–110.

[44] J. Zhang, Y.-S. Hu, J.-P. Tessonnier, G. Weinberg, J. Maier, R. Schlögl, D. S. Su, *Adv. Mater.* **2008**, *20*, 1450–1455.

[45] Y.-S. Hu, X. Liu, J.-O. Müller, R. Schögl, J. Maier, D. S. Su, *Angew. Chem. Int. Ed.* **2009**, *48*, 210–214.

[46] Y.-G. Guo, Y.-S. Hu, W. Sigle, J. Maier, *Adv. Mater.* **2007**, *19*, 2087–2091.

[47] Y.-S. Hu, Y.-G. Guo, R. Dominko, M. Gaberscek, J. Jamnik, J. Maier, *Adv. Mater.* **2007**, *19*, 1963–1966.

[48] I. Moriguchi, R. Hidaka, H. Yamada, T. Kudo, H. Murakami, N. Nakashima, *Adv. Mater.* **2006**, *18*, 69–73.

[49] D.-H. Lee, J.-G. Park, K. J. Choi, H.-J. Choi, D. W. Kim, *Eur. J. Inorg. Chem.* **2008**, 878–882.

[50] J. Yan, H. Song, S. Yang, J. Yan, X. Chen, *Electrochim. Acta* **2008**, *53*, 6351–6355.

[51] J. Li, S. Tang, L. Lu, H. C. Zeng, *J. Am. Chem. Soc.* **2007**, *129*, 9401–9409.

[52] H. Duan, X. Chen, J. Gnanaraj, J. Liang, "Electrochemical Preparation of Nanostructured $TiO_2$ As Anode Materials for Li Ion Batteries", *Materials Research Society Symposium Proceedings*, **2009**, 1127E(Mobile Energy), Paper: 1127-T01–02.

[53] M.-C. Tsai, J.-C. Chang, H.-S. Sheu, H.-T. Chiu, C.-Y. Lee, *Chem. Mater.* **2009**, *21*, 499–505.

[54] L. J. Hardwick, M. Holzapfel, P. Novak, L. Dupont, E. Baudrin, *Electrochim. Acta* **2007**, *52*, 5357–5367.

[55] S.-J. Bao, Q.-L. Bao, C.-M. Li, Z.-L. Dong, *Electrochem. Commun.* **2007**, *9*, 1233–1238.

[56] D. Wang, D. Choi, Z. Yang, V. V. Viswanathan, Z. Nie, C. Wang, Y. Song, J.-G. Zhang, J. Liu, *Chem. Mater.* **2008**, *20*, 3435–3442.

[57] M. Wagemaker, W. J. H. Borghols, E. R. H. van Eck, A. P. M. Kentgens, G. J. Kearleya, F. M. Mulder, *Chem. Eur. J.* **2007**, *13*, 2023–2028.

[58] R. Steiger, R. Beer, J. F. Fernandez-Sanchez, U. E. Spichiger-Keller, *Diffusion and Defect Data – Solid State Data, Part B: Solid State Phenomena*, **2007**, *121–123* (Nanoscience and Technology, Part 2), 1193–1197.

[59] N. Zhao, L. Fu, L. Yang, T. Zhang, G. Wang, Y. Wu, T. van Ree, *Pure Appl. Chem.* **2008**, *80*, 2283–2295.

[60] J. M. Zheng, J. Li, Z. R. Zhang, X. J. Guo, Y. Yang, *Solid State Ionics* **2008**, *179*, 1794–1799.

[61] A. Chen, X. Peng, P. Holt-Hindle, "$TiO_2$ Nanostructured Materials: Design, Characterization and Applications" in *Frontal Nanotechnology Research* (Ed.: M. V. Berg), Nova Science Publishers, Inc., Hauppauge, N. Y, **2007**, pp. 131–160.

[62] X. Chen, S. S. Mao, *J. Nanosci. Nanotechnol.* **2006**, *6*, 906–925.

[63] C. A. Grimes, *J. Mater. Chem.* **2007**, *17*, 1451–1457.

[64] G. K. Mor, O. K. Varghese, M. Paulose, K. Shankar, C. A. Grimes, *Sol. Energy Mater. Sol. Cells* **2006**, *90*, 2011–2075.

[65] Q. Chen, L.-M. Peng, *Int. J. Nanotechnol.* **2007**, *4*, 44–65.

[66] D. V. Bavykin, J. M. Friedrich, F. C. Walsh, *Adv. Mater.* **2006**, *18*, 2807–2824.

[67] F. Cheng, J. Chen, *J. Mater. Res.* **2006**, *21*, 2744–2757.

[68] Y.-K. Zhou, L. Cao, F.-B. Zhang, B.-L. He, H.-L. Li, *J. Electrochem. Soc.* **2003**, *150*, A1246–A1249.

[69] M. A. Khan, H.-T. Jung, O.-B. Yang, *J. Phys. Chem. B* **2006**, *110*, 6626–6630.

[70] Z. R. Tian, J. A. Voigt, J. Liu, B. Mckenzie, H. Xu, *J. Am. Chem. Soc.* **2003**, *125*, 12384–12385.

[71] J. M. Macak, H. Tsuchiya, A. Ghicov, K. Yasuda, R. Hahn, S. Bauer, P. Schmuki, *Curr. Opin. Solid State Mater. Sci.* **2007**, *11*, 3–18.

[72] O. K. Varghese, C. A. Grimes, *J. Nanosci. Nanotechnol.* **2003**, *3*, 277–293.

[73] O. K. Varghese, C. A. Grimes, *Sol. Energy Mater. Sol. Cells* **2008**, *92*, 374–384.

[74] S. Perathoner, R. Passalacqua, G. Centi, D. S. Su, G. Weinberg, *Catal. Today* **2007**, *122*, 3–13.

[75] S. Perathoner, R. Passalacqua, G. Centi, D. S. Su, G. Weinberg, *Studies in Surface Science and Catalysis*, **2007**, 172 (Science and Technology in Catalysis 2006), 437–440.

[76] G. Centi, S. Perathoner, "Opportunities and Problems in Developing an Advanced Nanoarchitecture in Metal-Oxide Catalysts" presented at the DICP Symposium (XVII) on Nanocatalysis, Dalian (China), July 9–12, **2008**.

[77] R. Hahn, A. Ghicov, H. Tsuchiya, J. M. Macak, A. G. Munoz, P. Schmuki, *Phys. Status Solidi A* **2007**, *204*, 1281–1285.

[78] D. Liu, P. Xiao, Y. Zhang, B. B. Garcia, Q. Zhang, Q. Guo, R. Champion, G. Cao, *J. Phys. Chem. C* **2008**, *112*, 11175–11180.

[79] J. Xu, C. Jia, B. Cao, W. F. Zhang, *Electrochim. Acta* **2007**, *52*, 8044–8047.

[80] G. F. Ortiz, I. Hanzu, T. Djenizian, P. Lavela, J. L. Tirado, P. Knauth, *Chem. Mater.* **2009**, *21*, 63–67.

[81] G. Centi, R. Passalacqua, S. Perathoner, D. S. Su, G. Weinberg, R. Schlögl, *Phys. Chem. Chem. Phys.* **2007**, *9*, 4930–4938.

[82] C. Ampelli, R. Passalacqua, S. Perathoner, G. Centi, D. S. Su, G. Weinberg, *Top. Catal.* **2008**, *50*, 133–144.

[83] Z. W. Zhao, Z. P. Guo, D. Wexler, Z. F. Ma, X. Wu, H. K. Liu, *Electrochem. Commun.* **2007**, *9*, 697–702.

[84] D. Fang, K. Huang, S. Liu, Z. Li, *J. Alloys Compd.* **2008**, *464*, L5–L9.

[85] B.-L. He, B. Dong, H.-L. Li, *Electrochem. Commun.* **2007**, *9*, 425–430.

[86] P. Poizot, S. Laruelle, S. Grugeon, L. Dupont, J. M. Tarascon, *Nature* **2000**, *407*, 496–499.

[87] H. K. Liu, G. X. Wang, Z. Guo, J. Wang, K. Konstantinov, *J. Nanosci. Nanotechnol.* **2006**, *6*, 1–15.

[88] F. Badway, I. Plitz, S. Grugeon, S. Laruelle, M. Dolle, A. S. Gozdz, J.-M. Tarascon, *Electrochem. Solid-State Lett.* **2002**, *5*, A115–A118.

[89] P. Poizot, S. Laruelle, S. Grugeon, L. Dupont, J.-M. Tarascon, *J. Power Sources* **2001**, *97–98*, 235–239.

[90] Z. Yang, D. Choi, S. Kerisit, K. M. Rosso, D. Wang, J. Zhang, G. Graff, J. Liu, *J. Power Sources* **2009**, *192*, 588–598.

[91] M. Wagemaker, E. R. H. van Eck, A. P. M. Kentgens, F. M. Mulder, *J. Phys. Chem. B* **2009**, *113*, 224–230.

[92] Z. Y. Zeng, J. P. Tu, X. L. Wang, X. B. Zhao, *J. Electroanal. Chem.* **2008**, *616*, 7–13.

[93] D. Wang, D. Choi, Z. Yang, V. V. Viswanathan, Z. Nie, C. Wang, Y. Song, J.-G. Zhang, J. Liu, *Chem. Mater.* **2008**, *20*, 3435–3442.

[94] P. Meduri, C. Pendyala, V. Kumar, G. U. Sumanasekera, M. K. Sunkara, *Nano Lett.* **2009**, *9*, 612–616.

[95] C.-C. Chang, S.-J. Liu, J.-J. Wu, C.-H. Yang, *J. Phys. Chem. C* **2007**, *111*, 16423–16427.

[96] Y. Liang, J. Fan, X.-h. Xia, Y.-s. Luo, Z.-j. Jia, *Electrochim. Acta* **2007**, *52*, 5891–5895.

[97] T. Cohen-Hyams, Y. V. Bhargava, S. A. Thorne, J. D. Wilcox, T. M. Devine, *ECS Trans.* **2008**, *11*, 1–7.

[98] L. C. Yang, Q. S. Gao, Y. Tang, Y. P. Wu, R. Holze, *J. Power Sources* **2008**, *179*, 357–360.

[99] M. V. Reddy, T. Yu, C.-H. Sow, Z. X. Shen, C. T. Lim, G. V. Rao, *Adv. Funct. Mater.* **2007**, *17*, 2792–2799.

[100] J. Chen, L. Xu, W. Li, X. Gou, *Adv. Mater.* **2005**, *17*, 582–586.

[101] Q. Fan, M. S. Whittingham, *Electrochem. Solid-State Lett.* **2007**, *10*, A48–A51.


  

[102] Y. H. Lee, I. C. Leu, C. L. Liao, S. T. Chang, M. T. Wu, J. H. Yen, K. Z. Fung, *Electrochem. Solid-State Lett.* **2006**, *9*, A207–A210.
[103] Y. Sharma, N. Sharma, G. V. S. Rao, B. V. R. Chowdari, *Electrochim. Acta* **2008**, *53*, 2380–2385.
[104] M. Van Thournout, L. Aldon, M. Womes, B. Ducourant, J. Olivier-Fourcade, C. Tessier, S. Levasseur, *J. Power Sources* **2007**, *174*, 1270–1274.
[105] M. V. Reddy, S. Madhavi, G. V. Subba Rao, B. V. R. Chowdari, *J. Power Sources* **2006**, *162*, 1312–1321.
[106] J.-S. Hu, L.-S. Zhong, W.-G. Song, L. J. Wan, *Adv. Mater.* **2008**, *20*, 2977–2982.
[107] L.-D. Zhang, X.-S. Fang, *J. Nanosci. Nanotechnol.* **2008**, *8*, 149–201.
[108] S.-M. Yang, S.-H. Kim, J.-M. Lim, G.-R. Yi, *J. Mater. Chem.* **2008**, *18*, 2177–2190.
[109] L. Lu, A. Eychmueller, *Acc. Chem. Res.* **2008**, *41*, 244–253.
[110] M.-O. Coppens, S. Gheorghiu, P. Pfeifer, *Studies in Surface Science and Catalysis*, **2005**, *156* (Nanoporous Materials IV), 371–378.
[111] B.-L. Su, A. Leonard, Z.-Y. Yuan, *C. R. Chim.* **2005**, *8*, 713–726.
[112] H. Yang, D. Zhao, *J. Mater. Chem.* **2005**, *15*, 1217–1231.
[113] C. Liang, Z. Li, S. Dai, *Angew. Chem. Int. Ed.* **2008**, *47*, 3696–3717.
[114] Y. Wan, Y. Shi, D. Zhao, *Chem. Mater.* **2008**, *20*, 932–945.
[115] H. Chang, S. H. Joo, C. Pak, *J. Mater. Chem.* **2007**, *17*, 3078–3088.
[116] J. Lee, J. Kim, T. Hyeon, *Adv. Mater.* **2006**, *18*, 2073–2094.
[117] R. Ryoo, S. H. Joo, M. Kruk, M. Jaroniec, *Adv. Mater.* **2001**, *13*, 677–681.
[118] F. Schüth, *Chem. Mater.* **2001**, *13*, 3184–3195.
[119] Q. Wang, D. F. Shantz, *J. Solid State Chem.* **2008**, *181*, 1659–1669.
[120] J. D. Holmes, M. A. Morris, K. M. Ryan, "Mesoporous Materials As Templates for Semiconductor Nanowire Assembly" in *Self-Assembly* (Ed.: B. H. Robinson), **2003**, IOS Press, Amsterdam, Netherlands, pp. 175–183.
[121] M. Casavola, R. Buonsanti, G. Caputo, P. D. Cozzoli, *Eur. J. Inorg. Chem.* **2008**, 837–854.
[122] M. Niederberger, *Acc. Chem. Res.* **2007**, *40*, 793–800.
[123] J. Eastoe, M. J. Hollamby, L. Hudson, *Adv. Colloid Interface Sci.* **2006**, *128–130*, 5–15.
[124] H. Boennemann, K. S. Nagabhushana, *Encyclopedia Nanosci. Nanotechnol.* **2004**, *1*, 777–813.
[125] A. T. Bell, *Science* (Washington, DC, US*)* **2003**, *299*, 1688–1691.
[126] R. Strobel, S. E. Pratsinis, *J. Mater. Chem.* **2007**, *17*, 4743–4756.
[127] M. Antonietti, M. Niederberger, B. Smarsly, *Dalton Trans.* **2008**, 18–24.
[128] M. O. Pileni, *J. Phys. Chem. C* **2007**, *111*, 9019–9038.
[129] P. D. Cozzoli, T. Pellegrino, L. Manna, *Chem. Soc. Rev.* **2006**, *35*, 1195–1208.
[130] S. Kinge, M. Crego-Calama, D. N. Reinhoudt, *ChemPhysChem* **2008**, *9*, 20–42.
[131] Y. Min, M. Akbulut, K. Kristiansen, Y. Golan, J. Israelachvili, *Nat. Mater.* **2008**, *7*, 527–538.
[132] M. Homberger, S. Karthaeuser, U. Simon, B. Voigtlaender, "Formation of Nanostructures by Self-Assembly" in *Nanotechnology* (Ed.: R. Waser), Wiley-VCH, Weinheim, Germany, **2008**, vol. 3, pp. 305–347.
[133] T. Umeyama, H. Imahori, *Energy Environ. Sci.* **2008**, *1*, 120–133.
[134] N. A. Kotov, "Layer-by-Layer Assembly of Nanoparticles and Nanocolloids: Intermolecular Interactions, Structure and Materials Perspectives" in *Multilayer Thin Films* (Eds.: G. Decher, J. B. Schlenoff), Wiley-VCH, Weinheim, Germany, **2003**, pp. 207–243.
[135] D. M. Lynn, *Adv. Mater.* **2004**, *16*, 1271–1293.
[136] S. Srivastava, N. A. Kotov, *Acc. Chem. Res.* **2008**, *41*, 1831–1841.
[137] M. Knez, *Mater. Matters* **2008**, *3*, 28–30.
[138] J. S. King, A. Wittstock, J. Biener, S. O. Kucheyev, Y. M. Wang, T. F. Baumann, S. K. Giri, A. V. Hamza, M. Baeumer, S. F. Bent, *Nano Lett.* **2008**, *8*, 2405–2409.
[139] J. W. Elam, J. A. Libera, M. J. Pellin, P. C. Stair, *Appl. Phys. Lett.* **2007**, *91*, 243105.
[140] Z. H. Barber, *J. Mater. Chem.* **2006**, *16*, 334–344.
[141] D. G. Schlom, L.-Q. Chen, X. Pan, A. Schmehl, M. A. Zurbuchen, *J. Am. Ceram. Soc.* **2008**, *91*, 2429–2454.
[142] A. Yasan, M. Razeghi, *Semiconductor Nanostructures for Optoelectronic Applications*, **2004**, 5–43.
[143] J. Bisquert, *Phys. Chem. Chem. Phys.* **2008**, *10*, 49–72.
[144] M. Quintana, T. Edvinsson, A. Hagfeldt, G. Boschloo, *J. Phys. Chem. C* **2007**, *111*, 1035.
[145] Y. Fukai, Y. Kondo, S. Mori, E. Suzuki, *Electrochem. Commun.* **2007**, *9*, 1439.
[146] D. Vanmaekelbergh, P. Liljerorth, *Chem. Soc. Rev.* **2005**, *34*, 299.
[147] D. Vanmaekelbergh, A. J. Houtepen, J. J. Kelly, *Electrochim. Acta* **2007**, *53*, 1140–1149.
[148] I. Heller, J. Kong, K. A. Williams, C. Dekker, S. G. Lemay, *J. Am. Chem. Soc.* **2006**, *128*, 7353–7359.
[149] P. G. Collins, M. S. Arnold, P. Avouris, *Science* **2001**, *292*, 706.
[150] H. J. Li, W. G. Lu, J. J. Li, X. D. Bai, C. Z. Gu, *Phys. Rev. Lett.* **2005**, *95*, 086601.
[151] C. P. Collier, T. Vossmeyer, J. R. Heath, *Annu. Rev. Phys. Chem.* **1998**, *49*, 371.
[152] J. B. Baxter, E. S. Aydil, *Appl. Phys. Lett.* **2005**, *86*, 053114.
[153] W.-S. Chae, S.-W. Lee, Y.-R. Kim, *Chem. Mater.* **2005**, *17*, 3072–3074.
[154] L. E. Greene, M. Law, D. H. Tan, M. Montano, J. Goldberger, G. Somorjai, P. Yang, *Nano Lett.* **2005**, *5*, 1231–1236.
[155] M. Law, L. E. Greene, A. Radenovic, T. Kuykendall, J. Liphardt, P. Yang, *J. Phys. Chem. B* **2006**, *110*, 22652–22663.
[156] G. K. Mor, K. Shankar, M. Paulose, O. K. Varghese, C. A. Grimes, *Nano Lett.* **2006**, *6*, 215–218.
[157] E. Palomares, J. N. Clifford, S. A. Haque, T. Lutz, J. R. Durrant, *J. Am. Chem. Soc.* **2003**, *125*, 475.
[158] F. Lenzmann, M. Nanu, O. Kijatkina, A. Belaidi, *Thin Solid Films* **2004**, *451–452*, 639.
[159] F. Fabregat-Santiago, J. García-Canãdas, E. Palomares, J. N. Clifford, S. A. Haque, J. R. Durrant, G. Garcia-Belmonte, J. Bisquert, *J. Appl. Phys.* **2004**, *96*, 6903.
[160] M. Law, L. E. Greene, A. Radenovic, T. Kuykendall, J. Liphardt, P. Yang, *J. Phys. Chem. B* **2006**, *110*, 22652.
[161] S. Ruhle, M. Greenshtein, S.-G. Chen, A. Merson, H. Pizem, C. S. Sukenik, D. Cahen, A. Zaban, *J. Phys. Chem. B* **2005**, *109*, 18907.
[162] Z. Zhang, S. M. Zakeeruddin, B. C. O'Regan, R. Humphry-Baker, M. Grätzel, *J. Phys. Chem. B* **2005**, *109*, 21818.
[163] Z. Zhang, N. Evans, S. M. Zakeeruddin, R. Humphry-Baker, M. Grätzel, *J. Phys. Chem. C* **2007**, *111*, 398.
[164] A. J. Nozik, *Inorg. Chem.* **2005**, *44*, 6893.
[165] R. J. Ellingson, M. C. Beard, J. C. Johnson, P. Yu, O. I. Micic, A. J. Nozik, A. Shabaev, A. L. Efros, *Nano Lett.* **2005**, *5*, 865.
[166] R. D. Schaller, M. Sykora, J. M. Pietryga, V. I. Klimov, *Nano Lett.* **2006**, *6*, 424.
[167] G. K. Mor, O. K. Varghese, M. Paulose, C. A. Grimes, *Adv. Funct. Mater.* **2005**, *15*, 1291–1296.
[168] H. E. Prakasam, K. Shankar, M. Paulose, O. K. Varghese, C. A. Grimes, *J. Phys. Chem. C* **2007**, *111*, 7235–7241.
[169] D. Kuang, J. Brillet, P. Chen, M. Takata, S. Uchida, H. Miura, K. Sumioka, S. M. Zakeeruddin, M. Grätzel, *ACS Nano* **2008**, *2*, 1113–1116.
[170] J. H. Park, S. Kim, A. J. Bard, *Nano Lett.* **2006**, *6*, 24–28.
[171] T. Sawatsuk, A. Chindaduang, C. Sae-kung, S. Pratontep, G. Tumcharern, *Diamond Relat. Mater.* **2009**, *18*, 524–527.

  

[172] D. Eder, A. H. Windle, *Adv. Mater.* **2008**, *20*, 1787–1793.
[173] M. Katayama, S.-i. Honda, T. Ikuno, K.-Y. Lee, M. Kishida, Y. Murata, K. Oura, *e-J. Surf. Sci. Nanotechnol.* **2004**, *2*, 244–255.
[174] L. Dai, *Adv. Appl. Ceram.* **2008**, *107*, 177–189.
[175] A. Huczko, *Appl. Phys. A: Mater. Sci. Proc.* **2002**, *74*, 617–638.
[176] I. Janowska, G. Wine, M. J. Ledoux, C. Pham-Huu, I. Janowska, G. Wine, M. J. Ledoux, C. Pham-Huu, *J. Mol. Catal. A* **2007**, *267*, 92–97.
[177] A. Kongkanand, P. V. Kamat, *ACS Nano* **2007**, *1*, 13–21.
[178] S. U. M. Khan, M. Al-Shahry, W. B. Ingler Jr, *Science* **2002**, *297*, 2243–2245.
[179] C. Pham-Huu, O. Ersen, M.-J. Ledoux, "Carbon and Silicon Carbide Nanotubes Containing Catalysts" in *Nanoparticles and Catalysis* (Ed.: D. Astruc), John Wiley & Sons **2007**, ch. 7, pp. 219–252.
[180] J.-Y. Gong, S.-R. Guo, H.-S. Qian, W.-H. Xu, S.-H. Yu, *J. Mater. Chem.* **2009**, *19*, 1037–1042.
[181] J. Bisquert, *J. Phys. Chem. B* **2004**, *108*, 2323.
[182] P. V. Kamat, *J. Phys. Chem. C* **2007**, *111*, 2834–2860.
[183] S. Chen, R. W. Murray, *J. Phys. Chem. B* **1999**, *103*, 9996–10000.
[184] K. P. Jayadevan, T. Y. Tseng, *J. Nanosci. Nanotechnol.* **2005**, *5*, 1768–1784.
[185] Y. Gao, M. Nagai, T.-C. Chang, J.-J. Shyue, *Cryst. Growth Des.* **2007**, *7*, 2467–2471.
[186] P. V. V. Jayaweera, A. G. U. Perera, K. Tennakone, *Inorg. Chim. Acta* **2008**, *361*, 707–711.
[187] R. Asahi, T. Morikawa, T. Ohwaki, K. Aoki, Y. Taga, *Science* **2001**, *293*, 269–271.
[188] A. Zaleska, *Recent Patents on Eng.* **2008**, *2*, 157–164.
[189] M. Ni, M. K. H. Leung, D. Y. C. Leung, K. Sumathy, *Renewable Sustainable Energy Rev.* **2007**, *11*, 401–425.
[190] S. In, A. Orlov, R. Berg, F. García, S. Pedrosa-Jimenez, M. S. Tikhov, D. S. Wright, R. M. Lambert, *J. Am. Chem. Soc.* **2007**, *129*, 13790–13791.
[191] H. A. Gasteiger, S. S. Kocha, B. Sompalli, F. T. Wagner, *Appl. Catal. B: Environ.* **2005**, *56*, 9.
[192] Y. Shao, J. Liu, Y. Wang, Y. Lin, *J. Mater. Chem.* **2009**, *19*, 46–59.
[193] A. L. Dicks, *J. Power Sources* **2006**, *156*, 128–141.
[194] D. Vairavapandian, P. Vichchulada, M. D. Lay, *Anal. Chim. Acta* **2008**, *626*, 119–129.
[195] J. Yan, H. Zhou, P. Yu, L. Su, L. Mao, *Adv. Mater.* **2008**, *20*, 2899–2906.
[196] Y. Shao, J. Sui, G. Yin, Y. Gao, *Appl. Catal. B: Env.* **2008**, *79*, 89–99.
[197] R. W. Murray, *Chem. Rev.* **2008**, *108*, 2688–2720.
[198] Y. Yamanoi, H. Nishihara, *Chem. Commun.* **2007**, 3983–3989.
[199] S. Sun, F. Jaouen, J.-P. Dodelet, *Adv. Mater.* **2008**, *20*, 3900–3904.
[200] Y. Shen, M. Träuble, G. Wittstock, *Anal. Chem.* **2008**, *80*, 750–759.
[201] H. Liu, L. Zhang, J. Zhang, D. Ghosh, J. Jung, B. W. Downing, E. Whittemore, *J. Power Sources* **2006**, *161*, 743–752.
[202] S. B. Adler, *Chem. Rev.* **2004**, *104*, 4791–4843.
[203] Y. Feng, N. Alonso-Vante, *Physica Status Solidi B* **2008**, *245*, 1792–1806.
[204] R. Zeis, T. Lei, K. Sieradzki, J. Snyder, J. Erlebacher, *J. Catal.* **2008**, *253*, 132–138.
[205] J. Maruyama, J. Okamura, K. Miyazaki, Y. Uchimoto, I. Abe, *J. Phys. Chem. C* **2008**, *112*, 2784–2790.
[206] J. Maruyama, I. Abe, *Chem. Commun.* **2007**, 2879–2881.
[207] P. Bert, C. Bianchini, Platinum-Free Electrocatalyst Materials for Fuel Cells, PCT Int. Appl. WO 2004036674, **2004**, assigned to Idea Lab S. R. L., Italy.
[208] P. Barbaro, P. Bert, C. Bianchini, G. Giambastiani, S. Moneti, A. Scaffidi, A. Tampucci, F. Vizza, Preparation and Use of Catalysts Based on Transition Metals for Fuel Cells, PCT Int. Appl. WO 2006063992, **2006**, assigned to Acta S. p. A., Italy.
[209] A. Witkowska, E. Principi, A. Di Cicco, S. Dsoke, R. Marassi, L. Olivi, M. Centazzo, A. R. Albertini, *J. Non-Cryst. Solids* **2008**, *354*, 4227–4232.
[210] M. Tada, S. Murata, T. Asakoka, K. Hiroshima, K. Okumura, H. Tanida, T. Uruga, H. Nakanishi, S.-i. Matsumoto, Y. Inada, M. Nomura, Y. Iwasawa, *Angew. Chem. Int. Ed.* **2007**, *46*, 4310–4315.
[211] H. Kageyama, T. Ioroi, T. Kojima, H. Senoh, N. Takeichi, K. Nomura, K. Tanimoto, "XAFS Analysis of Pt and Pt-Ru Catalysts for PEFCs by In-Situ Measurements under Operating Conditions in the Fluorescence Mode", *AIP Conference Proceedings*, **2007**, *882*[X-ray Absorption Fine Structure (XAFS13)], 645–647.
[212] S. Mukerjee, J. Ziegelbauer, T. Arruda, D. Ramaker, B. Shyam, *Electrochem. Soc. Interface* **2008**, *17*, 46–52.
[213] M. Teliska, V. S. Murthi, S. Mukerjee, D. E. Ramaker, *J. Phys. Chem. C* **2007**, *111*, 9267.
[214] A. Y. Lozovoi, A. Alavi, *Phys. Rev. B* **2003**, *68*, 245416.
[215] C. A. Lucas, N. M. Marković, P. N. Ross, *Phys. Rev. Lett.* **1996**, *77*, 4922–4925.
[216] L. L. Wang, D. D. Johnson, *J. Am. Chem. Soc.* **2007**, *129*, 3658–3664.
[217] L.-L. Wang, S. V. Khare, V. Chirita, D. D. Johnson, A. A. Rockett, A. I. Frenkel, N. H. Mack, R. G. Nuzzo, *J. Am. Chem. Soc.* **2006**, *128*, 131–142.
[218] B. Louis, D. Begin, M. J. Ledoux, C. Pham-Huu, "Advances in the Use of Carbon Nanomaterials in Catalysis" in *Ordered Porous Solids* (Eds.: V. Valtchev, S. Mintova, M. Tsapatsis), **2009**, Elsevier, Oxford, UK, pp. 621–649.
[219] K. P. D. Jong, J. W. Geus, *Catal. Rev. Sci. Eng.* **2000**, *42*, 481.
[220] Z. R. Ismagilov, M. A. Kerzhentsev, N. V. Shikina, A. S. Lisitsyn, L. B. Okhlopkova, Ch. N. Barnakov, M. Sakashita, T. Iijima, K. Tadokoro, *Catal. Today* **2005**, *102*, 58.
[221] J. H. Zhou, Z. J. Sui, P. Li, D. Chen, Y. C. Dai, W. K. Yuan, *Carbon* **2006**, *44*, 3255–3262.
[222] J. S. Zheng, X. S. Zhang, P. Li, J. Zhu, X. G. Zhou, W. K. Yuan, *Electrochem. Commun.* **2007**, *9*, 895–900.
[223] J. S. Zheng, X.-S. Zhang, P. Li, X. G. Zhou, W. K. Yuan, *Catal. Today* **2008**, *131*, 270–277.
[224] M. Tsuji, M. Kobokawa, T. Yano, N. Miyamae, T. Tsui, M. S. Jun, S. Hong, S. Lim, S. H. Yoon, I. Mochida, *Langmuir* **2007**, *23*, 387–390.
[225] M. Takasaki, Y. Motoyama, K. Higashi, S.-H. Yoon, I. Mochida, H. Nagashima, *Chem. Asian J.* **2007**, *2*, 1524–1533.
[226] A. T. Masheter, L. Xiao, G. G. Wildgoose, A. Crossley, J. H. Jones, *J. Mater. Chem.* **2007**, *17*, 3515–3524.
[227] E. S. Steigerwalt, G. A. Deluga, C. M. Lukehart, *J. Phys. Chem. B* **2002**, *106*, 760–766.
[228] T. Kim, S. Lim, K. Kwon, S. H. Hong, W. Qiao, C. K. Rhee, S. H. Yoon, I. Mochida, *Langmuir* **2006**, *22*, 9086–9088.
[229] P. Li, Q. Zhao, X. Zhou, W. Yuan, D. Chen, *J. Phys. Chem. C* **2009**, *113*, 1301–1307.
[230] S. Perathoner, M. Gangeri, P. Lanzafame, G. Centi, *Kinet. Catal.* **2007**, *48*, 877–883.
[231] S. Perathoner, G. Centi, M. Gangeri, *Chimica e l'Industria* (Milan, Italy), **2006**, *88*, 28–36.
[232] M. Gangeri, S. Perathoner, G. Centi, *Inorg. Chim. Acta* **2006**, *359*, 4828–4832.
[233] G. Centi, S. Perathoner, *Top. Catal.* **2009**, *52*, 948–961.
[234] G. Centi, M. Gangeri, M. Fiorello, S. Perathoner, J. Amadou, D. Bégin, M. J. Ledoux, C. Pham-Huu, M. E. Schuster, D. S. Su, J.-P. Tessonnier, R. Schlögl, *Catalysis Today*, **2009**, in press.
[235] J.-H. Ahn, H.-S. Shin, Y.-J. Kim, H. Chung, *J. Alloys Compd.* **2007**, *434–435*, 428.
[236] C. Xu, J. Chen, Y. Cui, Q. Han, H. Choo, P. K. Liaw, D. Wu, *Adv. Eng. Mater.* **2006**, *8*, 73.
[237] Z. Osváth, G. Vértesy, L. Tapasztó, F. Wéber, Z. E. Horváth, J. Gyulai, L. P. Biró, *Phys. Rev. B* **2005**, *72*, 045429.


  

[238] K.-D. Cai, G.-P. Yin, J.-J. Wang, K.-L. Lu, *Energy Fuels* **2009**, *23*, 903.
[239] A. Pozio, M. D. Francesco, A. Cemmi, F. Cardellini, I. Giorgi, *J. Power Sources* **2002**, *105*, 13.
[240] J. Maruyama, I. Abe, *Electrochim. Acta* **2001**, *46*, 3381.
[241] M. S. Saha, R. Li, X. Sun, *J. Power Sources* **2008**, *7*, 314.
[242] X. Cheng, Z. Shi, N. Glass, L. Zhang, J. Zhang, D. Song, Z.-S. Liu, H. Wang, J. Shen, *J. Power Sources* **2007**, *165*, 73.
[243] T. R. Ralph, M. P. Hogarth, *Platinum Met. Rev.* **2002**, *46*, 117.
[244] R. Borup, J. Meyers, B. Pivovar, Y. S. Kim, R. Mukundan, N. Garland, D. Myers, M. Wilson, F. Garzon, D. Wood, P. Zelenay, K. More, K. Stroh, T. Zawodzinski, J. Boncella, J. E. McGrath, M. Inaba, K. Miyatake, M. Hori, K. o. Ota, Z. Ogumi, S. Miyata, A. Nishikata, Z. Siroma, Y. Uchimoto, K. Yasuda, K.-i. Kimijima, N. Iwashita, *Chem. Rev.* **2007**, *107*, 3904–3951.
[245] Y. Y. Shao, G. Y. Z. Gao, *J. Power Sources* **2007**, *171*, 558–566.
[246] Y. Y. Shao, G. P. Yin, J. Zhang, Y. Z. Gao, *Electrochim. Acta* **2006**, *51*, 5853–5857.
[247] Y. Y. Shao, G. P. Yin, Y. Z. Gao, P. F. Shi, *J. Electrochem. Soc.* **2006**, *153*, A1093–A1097.
[248] L. Li, Y. C. Xing, *J. Electrochem. Soc.* **2006**, *153*, A1823–A1828.
[249] P. J. Ferreira, G. J. la O', Y. Shao-Horn, D. Morgan, R. Makharia, S. Kocha, H. A. Gasteiger, *J. Electrochem. Soc.* **2005**, *152*, A2256–A2271.
[250] J. G. Zhou, X. T. Zhou, X. H. Sun, R. Y. Li, M. Murphy, Z. F. Ding, X. L. K. Sun, T. K. Sham, *Chem. Phys. Lett.* **2007**, *437*, 229–232.
[251] C. Grolleau, C. Coutanceau, F. Pierre, J. M. Leger, *Electrochim. Acta* **2008**, *53*, 7157–7165.
[252] H. J. Kim, Y. S. Kim, M. H. Seo, S. M. Choi, W. B. Kim, *Electrochem. Commun.* **2009**, *11*, 446–449.
[253] X. Zhang, W. Lu, J. Da, H. Wang, D. Zhao, P. A. Webley, *Chem. Commun.* **2009**, 195–197.
[254] Y. Zhong, C. L. Xu, L. B. Kong, H. L. Li, *Appl. Surf. Sci.* **2008**, *255*, 3388–3393.
[255] H. Wang, C. Xu, F. Cheng, M. Zhang, S. Wang, S. P. Jiang, *Electrochem. Commun.* **2008**, *10*, 1575–1578.
[256] S. M. Choi, J. H. Kim, J. Y. Jung, E. Y. Yoon, W. B. Kim, *Electrochim. Acta* **2008**, *53*, 5804–5811.
[257] W. C. Choi, S. I. Woo, *J. Power Sources* **2003**, *124*, 420–425.
[258] G. Y. Zhao, C. L. Xu, D. J. Guo, H. Li, H. L. Li, *Appl. Surf. Sci.* **2007**, *253*, 3242–3246.
[259] Z. Chen, M. Waje, W. Li, Y. Yan, *Angew. Chem. Int. Ed.* **2007**, *46*, 4060–4063.

Received: March 23, 2009
Published Online: July 28, 2009

  